INSIDE

Stadtwerke München GmbH
Innovative Energie Pullach
Karlsruher Institut für Technologie

Karlsruhe Institute of Technology

Verbundvorhaben: Induzierte Seismizität & Bodendeformation als Interferenzaspekte beim Betrieb von Geothermieanlagen in der süddeutschen Molasse – Untersuchungen zu einem ver-besserten Prozessverständnis im tiefen Untergrund und Maßnahmen zur Risikominimierung

INSIDE SEISMIC MONITORING: METHODOLOGY AND RESULTS

The authors are responsible for the content of this publication

Title:	INSIDE seismic monitoring: Methodology and results
Work package:	AP3: Monitoring und Datenbearbeitung
Milestone:	M3.1.1
Due date:	-
Date:	-
Partner:	In charge: KIT
Contact person:	Jerome Azzola Email: jerome.azzola@kit.edu
Authors:	KIT : Jérôme Azzola, Emmanuel Gaucher
Version:	2.0

Version	Datum	Description of additions, changes, revisions
1.0	13.12.2024	First version
2.0	08.01.2025	After internal review (E. Gaucher)

TABLE OF CONTENTS

LIST OF FIGURES

Figure 1: Overview of the monitoring network in the south of Munich. The black lines depict the projection on the surface of the borehole trajectories at the Pullach and Schäftlarnstraße sites. White diamonds mark the locations of the INSIDE seismic monitoring stations, while green diamonds denote the positions of the stations of the BayernNetz operated by the Geophysical Observatory Fürstenfeldbruck (GOF)/ LMU. 9

LIST OF TABLES

1 INTRODUCTION

The INSIDE project aims to improve the understanding of induced seismicity and ground deformation associated with geothermal operations in the South German Molasse Basin. The seismic monitoring network deployed in the frame of the project plays a crucial role in achieving this objective. This technical report focuses on the passive seismic monitoring efforts conducted in the southern Munich area, Germany, between March 2021 and January 2024.

This document details the equipment and the focus of the monitoring, specifically the geothermal activity in the southern Munich area around the ongoing Pullach and Schäftlarnstraße sites, as well as the future Baierbrunn project. The report presents a catalogue of seismic events detected between March 2021 and December 2023, comparing the findings with data from the Geophysical Observatory Fürstenfeldbruck (GOF). It analyses data quality, signal-to-noise ratios and develops on the accuracy of hypocenter determination. It focuses on different location methods (absolute and relative), tests the hypothesis underlying the development of the velocity models and develops on the influence of the seismic network geometry. Finally, the report validates the simulated network capabilities from the observed catalogue.

Further details regarding the methods used and the scientific context underlying these results are described in Section 10. In the following, we use these conventions:

- DHDN / 3-degree Gauss-Kruger zone 4 ("GK4") coordinate system (EPSG 31468),
- Vertical coordinates are considered positive below MSL.

2 THE INSIDE SEISMIC MONITORING NETWORK

2.1 OVERVIEW

The seismic monitoring network deployed in the framework of the INSIDE project focuses on the passive seismic monitoring of the southern part of the Munich area, with a particular focus on the currently operated Pullach and Schäftlarnstraße sites, as well as on the future Baierbrunn site. Five sites were selected over the study area for the installation of monitoring instruments in a variety of setups and configurations. The monitoring network includes:

- Four surface stations. The associated station names are WBRU, FRIE, FROS and BUCH.
- One borehole station in Siemensallee. The associated station name is SIEM.
- One Distributed Fiber Optic Sensing (DFOS) station in Buchenhain. It includes a dedicated monitoring borehole (up to about 250 m) and a section of fiber optic cables deployed twice around a 80-m long loop close to surface.
- Mini-Array with nine geophones / stations in the Siemens Park.

In Table 1, we list the different types of seismic stations and the associated sensor(s).

Table 1: Types of seismic stations that have been installed at the selected monitoring sites.

Location of station	Station ID	Surface	Borehole	Fiber Optic Sensing	Mini-Array
Waldfriedhof (Neuried)	FRIE	1 Trillium Compact Vault 120s			
Wörnbrunn (Grünwald)	WBRU	1 Trillium Compact Vault 120s			
Forstenriede Park	FORS	1 Trillium Compact Vault 120s			
Buchenhain	BUCH	1 Trillium Compact Vault 120s		DAS + DTSS	
Siemensallee (Sendling)	SIEM		1 Trillium Compact Posthole 20s		9 geophones

2.2 LOCATIONS

Table 2 provides further details on the measurement stations, including their location, date of commissioning and recording parameters.

Table 2: Location and start of operation of the different monitoring stations installed within the INSIDE project.

Surface and borehole seismometer stations

Seismometer station	BUCH	WBRU	SIEM	FORS	FRIE
Easting [m]	4461914	4466521	4465091	4458486	4461772
Northing [m]	5321385	5322589	5327929	5325249	5329311
Commissioning	10 June 2021	27 March 2021	26 Nov. 2020	28 March 2021	28 March 2021
Sampling (Hz)	250				

Mini-array in Siemens Park

Mini array station	Easting [m]	Northing [m]	Sampling (Hz)	Commissioning
S1	4464513	5327891	200	11.05.2022
S2	4464664	5328310	200	11.05.2022
S3	4464392	5327758	200	11.05.2022
S4	4465091	5327930	250	11.05.2022
S5	4464791	5328136	200	11.05.2022
S6	4464860	5327978	200	11.05.2022
S7	4464643	5328072	200	11.05.2022
S8	4464743	5328008	200	11.05.2022
S9	4464859	5328067	200	11.05.2022

DFOS station

Buchenhain (DFOS)	Easting [m]	Northing [m]	Sampling (Hz)	Commissioning
Wellhead	4461916	5321379	500	06.2021
Near surface loop	2 loops of FOC around a parc in the Buchenhain municipality		500	06.2021

Figure 1 (white dots) shows the final locations of the seismic stations part of the INSIDE monitoring network on a map of the study area. To show how these stations fit into the larger operator network, the map also includes the surrounding stations of the BayernNetz (green dots) (Department of Earth and Environmental Sciences, Geophysical Observatory, University of Munchen, 2001). The recordings of the public stations MGS0* and UH3 operated near the INSIDE network are used for event location. Figure 1 also includes the surface projection of the trajectories of the Pullach and Schäftlarnstraße wells to locate the seismic stations in relation to the sites under focus.
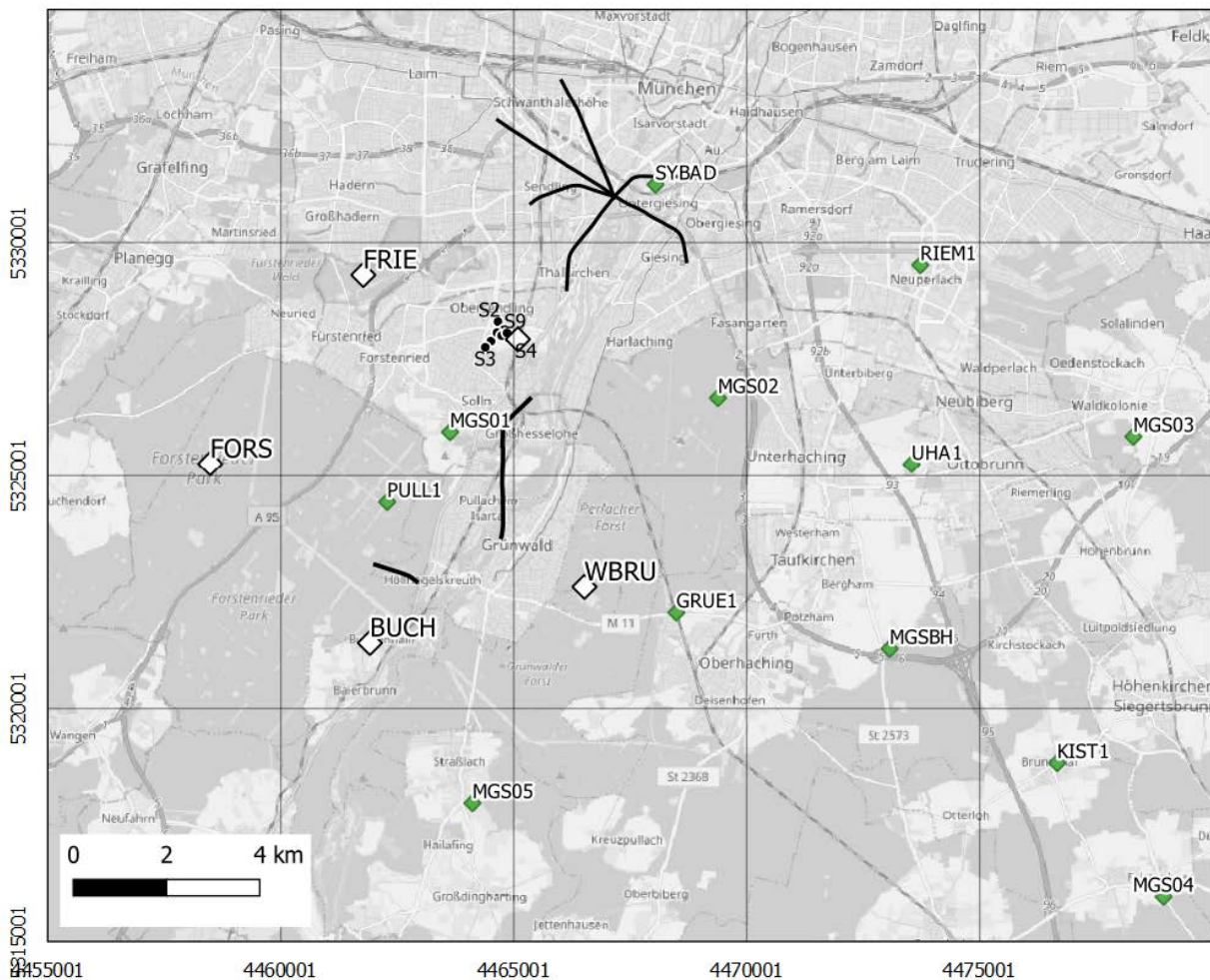
Figure 1: Overview of the monitoring network in the south of Munich. The black lines depict the projection on the surface of the borehole trajectories at the Pullach and Schäftlarnstraße sites. White diamonds mark the locations of the INSIDE seismic monitoring stations, while green diamonds denote the positions of the stations of the BayernNetz operated by the Geophysical Observatory Fürstenfeldbruck (GOF)/ LMU.

Figure 2 focuses on monitoring capabilities deployed at the Siemensallee and in Buchenhain, where multiple types of instruments have been installed at the same location. Figure 2 (b) shows the location of the nine stations of the Siemens Park mini-array that is deployed at the same location as the borehole sensor "SIEM". Figure 2 (c) focuses on the Buchenhain monitoring site. In addition to the surface seismometer "BUCH", fiber optic cables were installed near surface (in a trench including two cable loops of ~90 m each) and in a 250 m deep well.
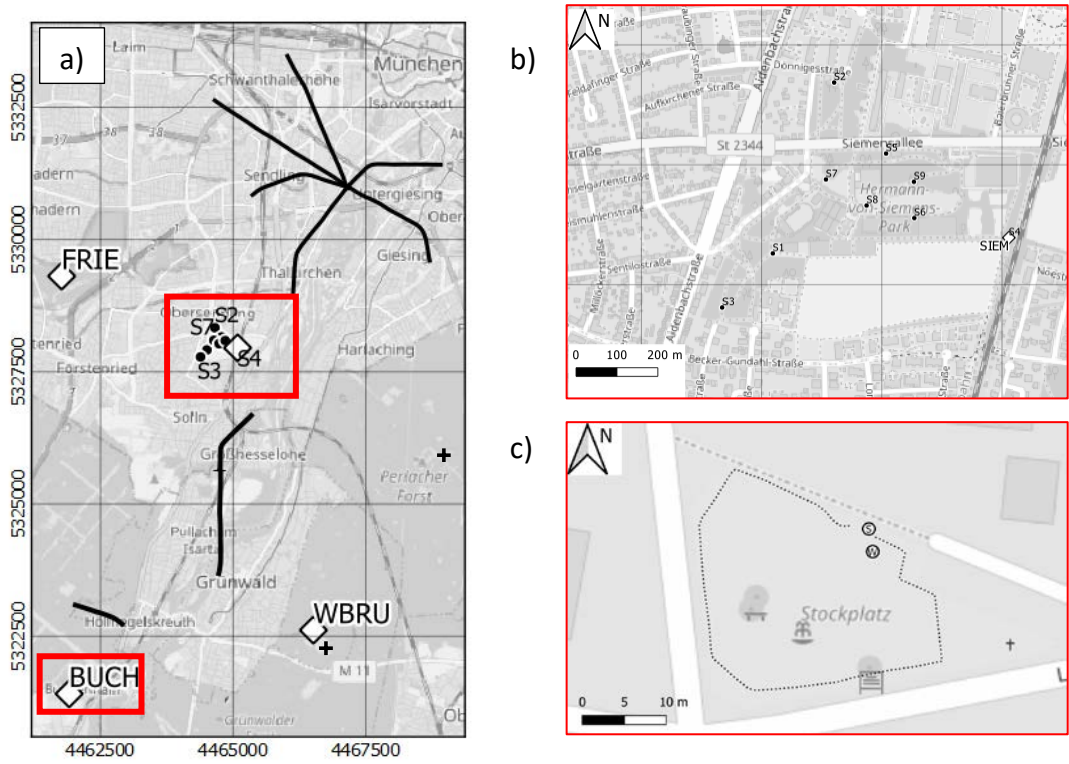
Figure 2: Maps focusing on the monitoring instruments deployed around Siemens Park (panel b) and in Buchenhain (panel c). The location of the 9 geophones is indicated by the black dots from S1 to S9 and in Buchenhain, the location of the well (W) and of the seismometer BUCH (S) is shown with the FOC near surface (black dots).

As illustrated in Figure 1 and Figure 2, the INSIDE "monitoring concept" includes multiple measurements locations, monitoring techniques and configurations. The goal of the mini-array and borehole stations is to achieve higher signal acquisition capability than with a single surface geophone. Furthermore, the suitability of fiber optic cables for recording seismic signals is evaluated during the project. Hence, by mixing recording techniques in the field, the methods can be compared and their advantages and disadvantages described. The objective of this monitoring concept is to evaluate these monitoring components regarding their suitability for monitoring local (micro-) seismicity. The comparison of measurement types and configuration is the focus of another report. In this context, establishing a reference catalogue of detected and described seismic events is crucial as it serves as a base for comparison purposes. The aim of this document is therefore to describe this reference catalogue.

3 DATA AVAILABILITY

3.1 SEISMOMETER NETWORK

Since commissioning, the seismometer network acquired data continuously with some downtime at the Forstenrieder-park (FORS) and Neuried (FRIE) stations (see Figure 3).

All seismometer stations are power by the electrical grid, except for the FORS one. These seismometer stations are equipped with uninterruptible power supply systems, providing backup power in case of grid power failure. Performing a quality check on the available datasets enables to evaluate the

completeness of the dataset (Figure 3). For that we use the scanning algorithm[1] available in the Obspy python library (Beyreuther et al., 2010). The gaps observed in Figure 3 are due to longer power shutdowns. At the FORS station, which is powered by solar panels, these downtimes are due to equipment theft (September 2022) or climatic conditions (during the winter).
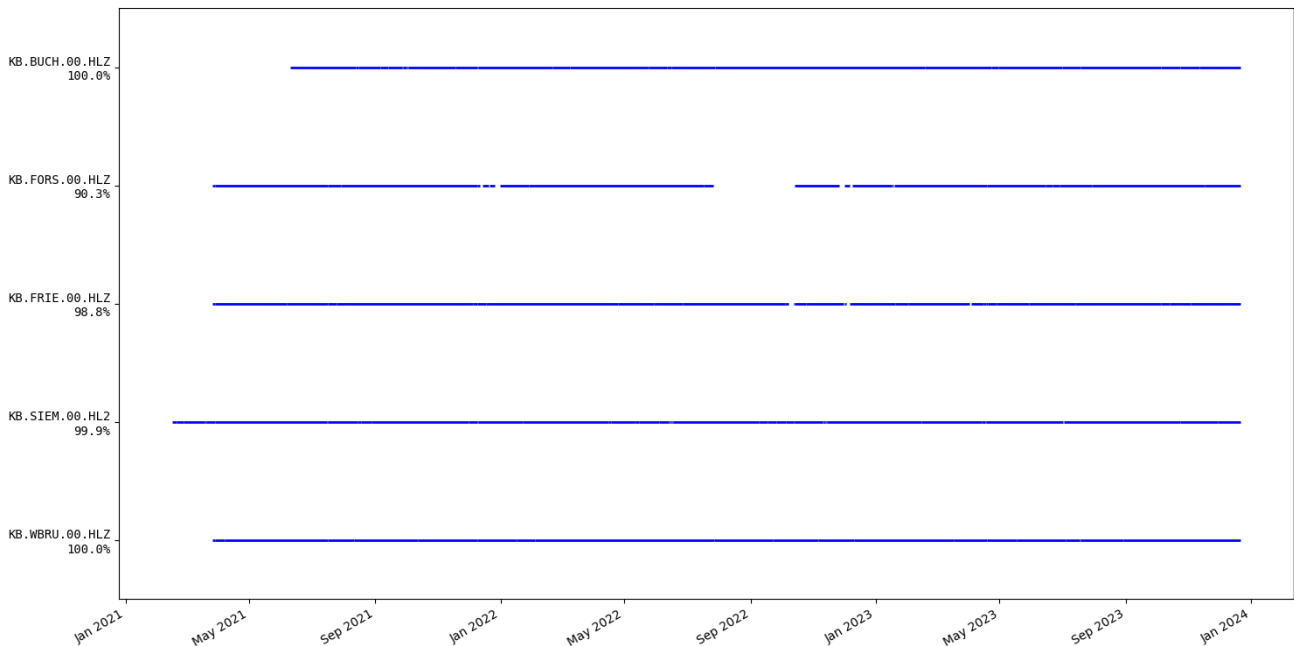
Figure 3: Result of a quality-check applied to the recordings of the seismometer stations. The blue lines indicate the data availability since network commissioning, in 2021. Each station is referenced according to the ID of a single channel.

3.2 SIEMENS PARK MINI-ARRAY

The Siemens Park mini-array was operated continuously from May 2021 to September 2023. The recordings were not transferred in real time to Karlsruhe but saved locally on 32 GB memory cards. This necessitates the establishment of a maintenance schedule for the stations, involving data uploading every three to four months and battery replacement every 6 months.

---

[1]*https://docs.obspy.org/packages/autogen/obspy.imaging.scripts.scan.html#module-obspy.imaging.scripts.scan*
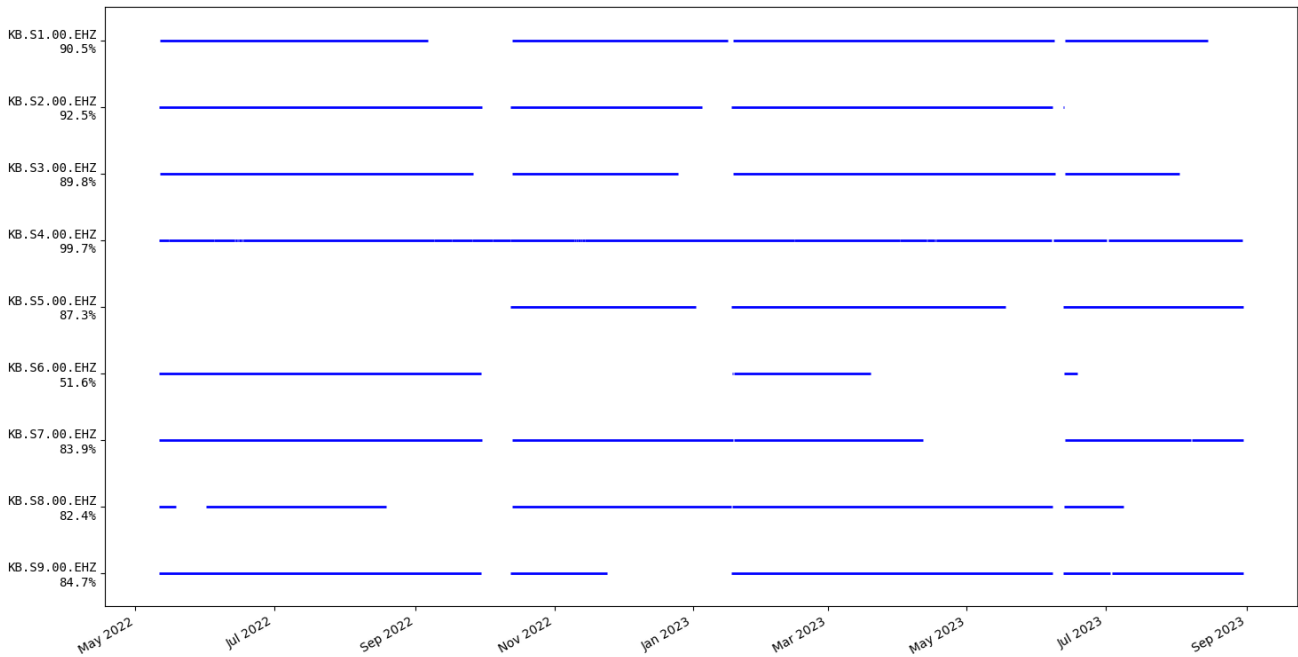
Figure 4: Results of a quality check applied to the recordings of the mini-array stations operated from May 2022 to September 2023 in the Siemens-park (Munich, Germany). The blue lines indicate the data availability for each station, referenced via the ID of a single channel.

The gaps observed in the dataset have multiple origins:

- the memory card was full before the maintenance,
- the battery was empty and the station no longer powered,
- water came inside the data logger and the data was lost,
- passers-by in the park found and removed the station.

These gaps affect data processing and limit network capacity. The traces acquired by the multiple stations of the array can be combined to reinforce the coherent signals while attenuating random noise (beamforming and stacking), as random noise tends to average out because it is not consistently present across all traces. In theory, an improvement of the SNR by square root the number of stations is expected by data processing. However, Figure 4 shows that the nine stations of the mini-array were not often operated all simultaneously.

3.3 DISTRIBUTED ACOUSTIC SENSING

In Buchenhain, DAS is operated continuously. In the same way as for the Siemens Park mini-array, the data are not transferred in real-time to Karlsruhe. The recordings are stored on a 24 TB data bay, which is transported to Karlsruhe to make a complete backup of acquired data files. Table 3 shows the data availability for the DAS measuring station.

Table 3: Availability of DAS-data from the Buchenhain station, with months of actual operation and data acquisition shown with a green background and starting dates indicated with green numbers.

2021											
1	2	3	4	5	6	7	8	9	10	11	12
						15>29	12>				

2022											
1	2	3	4	5	6	7	8	9	10	11	12
>25		25>									

2023											
1	2	3	4	5	6	7	8	9	10	11	12
		>27		23>							

RAW (non-converted to SR) data
10 June 2021
14, 15 July 2021
10, 11 and 12-Aug. 2021 (PULL TH3 VSP + Hammer Tests)
06 October 2021
23, 24, 25 March 2022

At the Buchenhain station, the larger downtimes in data acquisition were related to hardware issues requiring the maintenance of the station. In parallel, smaller downtimes of a few minutes are experienced because of disconnections from the GPS network for time-stamping data.

In addition, DAS was operated continuously in Schäftlarnstraße from February to August 2022 on the TH3 fiber optic cable. The DAS continuous power supply was ensured by using a UPS and data were transferred in real time to the MS Azure cloud, on a Data Lake. During the 6-month passive monitoring period, 4137 files have been uploaded to the Azure Data Lake used for the long-term storage of the data. They represent a ~20 549 GB large dataset, representing 4077 hours of recordings. The recording had some interruptions during the 6 months with in total, an 8.53 GB data gap, corresponding to ~ 1.7 hours of recording. The monitoring results associated with the 6-month survey are not detailed in this document, but are the focus of peer-reviewed articles by (Azzola et al., 2023; Azzola and Gaucher, 2024).

4   DETECTION OF SEISMIC EVENTS

4.1   CATALOG OF DETECTED EVENTS

Table 4 details all seismic events detected during the operation of the seismometer network installed within INSIDE from March 2021 (commissioning of the INSIDE seismometer network) to end of December 2023. The seismic events detection is based on the workflow described in Section 10.1.

The catalogue shows first the trigger time of each detected event that was validated after visual inspection in Snuffler (see workflow Section 10.1). It also provides an indicator of the signal quality on the INSIDE network. The second column shows if the signal to noise ratio (SNR) observed on individual stations of the network allows locating the event (light green background), i.e. if the observed seismic signal allows collecting 3 arrival times on 3 distinct stations.

The table also shows results from the template matching analysis. It details the template waveform giving the highest correlation with the triggered data, along with the maximum correlation coefficient and matching channel SEED ID[2]. This correlation analysis results in the assignment of the detection to a cluster. This preliminary location is deduced from the one of the templates with highest correlation value. The background colors distinguish events from the two sites where a major part of the seismicity was observed. A light blue (or light red) background indicates that the seismic event is linked to the Unterhaching (or Oberhaching) sites. Finally, we present the detections observed and reported by the Geophysical Observatory (Tobias Megies, personal communication) for the corresponding period.

Several comments and conclusions can be drawn from Table 4.

- Most of the detected events are linked to the Oberhaching site (49 detections from the INSIDE network, out of 79) and the Unterhaching site (27 detections).
- 12 events (6 "Oberhaching" and 6 "Unterhaching" events) are reported by the seismological services and not detected by the INSIDE network. The positioning of the WBRU (and to a lesser extent, BUCH) station in relation to the trajectories of the Unterhaching boreholes allows for the identification of additional unreported events (3 "Oberhaching", 8 "Unterhaching" events and 1 located near Pullach TH3). This implies the complementary role of these stations in seismic monitoring within the study area.
- The rough origin suggested by the template analysis is consistent with the results provided by the seismological services. It shows that the templates collected for these sites faithfully represent the signals collected and associated with the events at these two sites. For illustration, we show the signals associated with Oberhaching, Unterhaching and Pullach events in Figure 5. The signals are recorded at the WBRU station in the 5-40 Hz frequency band. Considering the observations made during the monitoring period, the high correlation coefficients noticed for the WBRU station, attributed to high signal-to-noise ratios, underscore the significance of the station in the application of template matching.
- Out of the 79 events, nine events are associated with insufficient data quality on the INSIDE stations, which prevents further analysis for event description purposes.
- Given the location of the INSIDE stations in relation to the Unterhaching and Oberhaching sites, the INSIDE network coverage is insufficient to yield reliable and precise locations for most of the detected events. Hence, the INSIDE recordings have been supplemented by recordings from the public stations of the BayernNetz (see Section 4 or 10.2).

---

[2] http://ds.iris.edu/ds/nodes/dmc/data/formats/miniseed/
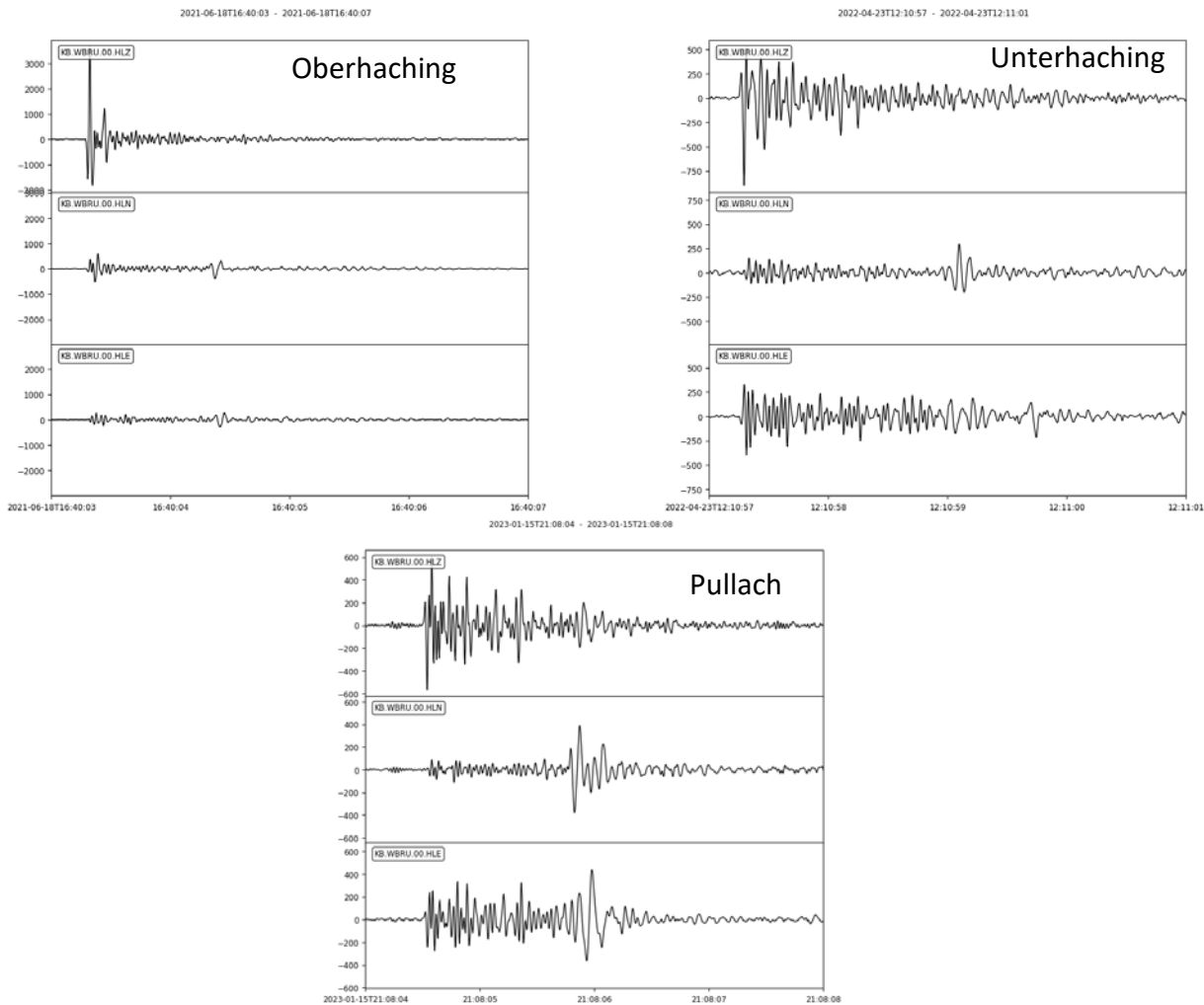
Figure 5: Example of seismic signals acquired on the 3C seismometer WBRU and filtered in the 5-40 Hz frequency band.

In addition, we note that events reported by the seismological services from other nearby sites (Duerrnhaar and Sauerlach) were not observed on the records of the INSIDE stations.

In the framework of the project, the catalogue of detected event shown in Table 4 consists in a reference that can be used:

- to evaluate the relevance of the velocity structures developed during the project and analyze the impact of specific velocity profiles on the inverted locations and the associated residuals/errors. (see Section 6).

- to evaluate the contribution of the Siemens-park mini-array and Buchenhain DAS station to the monitoring (see Section 4.3 and dedicated report).

These lines of analysis are further exploited in the following and in the report focusing on the comparison of monitoring capabilities of different monitoring infrastructures.

Table 4: Catalog of detected seismic events, from March 2021 (start of the operation of the INSIDE seismometer network) to the end of December 2023. The table presents, from left to right, the time at which the seismometer network triggers the seismic events. Then, an evaluation is conducted to determine if the Signal-to-Noise Ratio (SNR) observed on the channels of the five INSIDE stations allows for event location: a light green background color indicates that a SNR of at least 3 was observed on a minimum of 3 INSIDE stations. Following this, results from the template matching analysis are displayed, with the cluster association suggested by the template analysis. Finally, the results communicated by local seismological services (Tobias Megies, personal communication) are presented, with light blue (or light red) background colors showing seismic events associated with the Unterhaching (or Oberhaching) sites.

Legend:

Observed SNR > 3 on channels of a minimum of 3 INSIDE stations
associated to Oberhaching
associated to Unterhaching

Trigger time (UTC)	INSIDE					LMU
	SNR evaluation	Max correlation coefficient …	… on channel …	… and template from event …	Origin (suggested by template)	Event reported and located
2021-03-05T21:56:23.24		0.85	WBRU.HLZ	2021-06-18T16:40:03	Oberhaching	Oberhaching
2021-03-30T00:34:54.28		0.93	WBRU.HLZ	2021-06-18T16:40:03	Oberhaching	Oberhaching
2021-04-04T09:10:36.02	not reported					Oberhaching
2021-06-04T14:55:57.89		0.75	BUCH.HLZ	2023-04-22T23:06:43	Other	Other
2021-06-08T05:42:51.00		0.86	WBRU.HLN	2022-03-08T03:56:33	Oberhaching	Oberhaching
2021-06-18T16:40:02.38		0.81	WBRU.HLZ	2022-08-11T10:15:02	Oberhaching	Oberhaching
2021-06-18T16:43:58.10		0.98	WBRU.HLZ	2021-06-18T16:40:03	Oberhaching	Oberhaching
2021-06-18T17:01:45.22		0.99	WBRU.HLZ	2021-06-18T16:40:03	Oberhaching	Oberhaching
2021-06-18T17:11:12.50	not reported					Oberhaching
2021-06-18T19:27:44.00		0.95	WBRU.HLN	2021-06-18T16:40:03	Oberhaching	Oberhaching
2021-06-19T01:40:37.00		0.83	WBRU.HLZ	2021-06-18T16:40:03	Oberhaching	Oberhaching
2021-06-19T02:13:32.11		0.81	WBRU.HLZ	2021-06-18T16:40:03	Oberhaching	Oberhaching
2021-10-22T17:55:02.50		0.81	SIEM.HL2	2021-10-22T23:21:44	Unterhaching	Unterhaching

Trigger time (UTC)	SNR evaluation	Max correlation coefficient …	… on channel …	… and template from event …	Origin (suggested by template)	Event reported and located
2021-10-22T23:21:43.00		0.95	WBRU.HLE	2021-10-23T04:52:43	Unterhaching	not reported
2021-10-23T03:05:39.60		0.95	WBRU.HLE	2021-10-28T21:49:09	Unterhaching	Unterhaching
2021-10-23T04:52:44.50		0.95	WBRU.HLE	2021-10-22T23:21:42	Unterhaching	not reported
2021-10-23T18:51:16.60		0.61	WBRU.HLZ	2021-06-04T14:55:59	Unterhaching	Unterhaching
2021-10-26T09:42:38.00		0.96	WBRU.HLE	2021-11-01T08:02:05	Unterhaching	Unterhaching
2021-10-28T21:49:11.80		0.95	WBRU.HLE	2021-10-23T03:05:37	Unterhaching	not reported
2021-11-01T08:02:07.50		0.96	WBRU.HLE	2021-10-26T09:42:36	Unterhaching	Unterhaching
2021-12-03T15:24:11.50		0.80	WBRU.HLZ	2021-06-18T16:40:03	Oberhaching	Oberhaching
2021-12-03T21:52:56.10		0.78	WBRU.HLN	2022-01-18T23:52:52	Unterhaching	Unterhaching
2022-01-18T23:52:53.50		0.59	SIEM.HL2	2021-10-22T23:21:44	Unterhaching	no reported
2022-02-09T05:51:32.00		0.89	WBRU.HLN	2022-02-09T11:48:54	Unterhaching	Unterhaching
2022-02-09T11:48:55.00		0.89	WBRU.HLN	2022-02-09T05:51:31	Unterhaching	Unterhaching
2022-03-01T05:25:33.00		0.89	WBRU.HLN	2022-02-09T05:51:31	Unterhaching	not reported
2022-03-06T03:58:59.50		0.74	WBRU.HLN	2022-03-08T03:56:33	Oberhaching	Oberhaching
2022-03-08T03:56:34.00		0.99	WBRU.HLN	2022-03-08T04:28:25	Oberhaching	Oberhaching
2022-03-08T04:28:26.00		0.99	WBRU.HLN	2022-03-08T03:56:33	Oberhaching	Oberhaching
2022-03-08T04:30:55.30		0.97	WBRU.HLN	2022-03-08T03:56:33	Oberhaching	Oberhaching
2022-04-16T11:39:19.00		0.83	WBRU.HLN	2022-03-08T03:56:33	Oberhaching	Oberhaching
2022-04-23T12:10:58.00		0.97	WBRU.HLN	2022-04-23T20:29:10	Unterhaching	Unterhaching
2022-04-23T20:29:10.20		0.97	WBRU.HLN	2022-04-23T12:10:57	Unterhaching	Unterhaching
2022-05-21T22:24:11.50		0.87	WBRU.HLZ	2021-06-18T16:40:03	Oberhaching	not reported
2022-05-21T23:14:04.00		0.86	WBRU.HLZ	2021-06-18T16:40:03	Oberhaching	Oberhaching
2022-05-21T23:48:19.50		0.78	WBRU.HLN	2022-03-08T03:56:33	Oberhaching	Oberhaching
2022-05-26T20:51:30.00		0.88	WBRU.HLZ	2023-03-09T01:21:33	Oberhaching	Oberhaching
2022-08-11T10:15:02.50		0.81	WBRU.HLZ	2021-06-18T16:40:03	Oberhaching	Oberhaching

Trigger time (UTC)	SNR evaluation	Max correlation coefficient …	… on channel …	… and template from event …	Origin (suggested by template)	Event reported and located
			INSIDE			**LMU**
2022-09-07T00:56:43.00		0.93	WBRU.HLE	2021-10-23T03:05:37	Unterhaching	**not reporte**d
2022-09-07T02:07:55.00		0.93	SIEM.HL2	2021-10-22T23:21:44	Unterhaching	**not reported**
2022-09-25T14:48:05.50		0.81	WBRU.HLN	2022-03-06T03:58:59	Oberhaching	Oberhaching
2022-12-05T22:35:52.20		0.93	WBRU.HLE	2021-10-23T03:05:37	Unterhaching	**not reported**
2022-12-09T03:21:41.50		0.80	WBRU.HLN	2022-03-08T03:56:33	Oberhaching	Oberhaching
2022-12-27T03:49:29.00		0.78	WBRU.HLZ	2023-03-06T08:52:14	Oberhaching	**not reported**
2023-01-15T21:08:04.00		0.71	WBRU.HLN	2022-03-08T04:28:25	Pullach (Th3)	**not reported**
2023-02-25T15:05:57.65	**not reported**					Oberhaching
2023-02-25T15:35:00.20		0.96	WBRU.HLZ	2023-03-06T08:52:14	Oberhaching	Oberhaching
2023-02-26T00:34:23.72	**not reported**					Oberhaching
2023-03-01T15:36:38.80		0.95	WBRU.HLZ	2023-03-06T08:52:14	Oberhaching	Oberhaching
2023-03-06T08:52:15.30		0.95	WBRU.HLZ	2023-03-01T15:36:38	Oberhaching	Oberhaching
2023-03-09T01:21:34.00		0.63	WBRU.HLZ	2023-03-06T08:52:14	Oberhaching	
2023-04-22T23:06:43.10		0.85	BUCH.HLZ	2021-06-04T14:55:58	Pullach (Th3)	Pullach (Th3)
2023-05-06T06:43:56.50		0.81	WBRU.HLZ	2023-03-01T15:36:38	Oberhaching	
2023-05-06T08:19:20.30		0.83	WBRU.HLZ	2023-03-01T15:36:38	Oberhaching	
2023-05-06T10:02:28.00		0.84	WBRU.HLZ	2023-03-06T08:52:14	Oberhaching	
2023-05-06T11:17:05.80		0.84	WBRU.HLZ	2023-03-06T08:52:14	Oberhaching	
2023-05-06T16:53:33.76		0.84	WBRU.HLZ	2023-03-06T08:52:14	Oberhaching	
2023-05-06T17:35:31.56		0.84	WBRU.HLZ	2023-03-01T15:36:38	Oberhaching	
2023-05-06T17:38:20.31		0.84	WBRU.HLZ	2023-03-01T15:36:38	Oberhaching	
2023-08-06T02:41:21.52		0.74	BUCH.HLN	2023-01-15T21:08:04	Oberhaching	Oberhaching
2023-08-06T02:51:48.98		0.7	BUCH.HLN	2023-01-15T21:08:04	Oberhaching	Oberhaching
2023-08-06T03:41:59.13		0.97	WBRU.HLZ	2021-06-18T16:40:03	Oberhaching	Oberhaching
2023-08-06T03:43:01.05		0.95	WBRU.HLZ	2021-06-18T16:40:03	Oberhaching	Oberhaching

Trigger time (UTC)	INSIDE					LMU
	SNR evaluation	Max correlation coefficient …	… on channel …	… and template from event …	Origin (suggested by template)	Event reported and located
2023-08-06T03:45:13.31		0.93	WBRU.HLZ	2021-06-18T16:40:03	Oberhaching	Oberhaching
2023-08-06T03:50:34.72		0.94	WBRU.HLZ	2021-06-18T16:40:03	Oberhaching	Oberhaching
2023-08-06T04:01:29.30		0.98	WBRU.HLZ	2021-06-18T16:40:03	Oberhaching	Oberhaching
2023-08-06T04:25:01.66		0.98	WBRU.HLZ	2021-06-18T16:40:03	Oberhaching	Oberhaching
2023-08-06T04:25:05.00		0.97	WBRU.HLZ	2021-06-18T16:40:03	Oberhaching	Oberhaching
2023-08-06T04:36:50.22	not reported					Oberhaching
2023-08-06T04:36:51.28		0.63	WBRU.HLN	2023-01-15T21:08:04	Oberhaching	Oberhaching
2023-08-06T04:58:06.84		0.97	WBRU.HLZ	2021-06-18T16:40:03	Oberhaching	Oberhaching
2023-08-06T04:58:39.66		0.85	BUCH:HLN	2023-01-15T21:08:04	Oberhaching	Oberhaching
2023-08-06T05:47:18.40		0.9	WBRU.HLZ	2021-06-18T16:40:03	Oberhaching	Oberhaching
2023-10-11T15:53:53.71	not reported					Oberhaching
2023-10-17T03:09:50.70		0.73	WBRU.HLN	2022-03-08T03:56:33	Unterhaching	Unterhaching
2023-10-20T13:12:54.28	not reported					Unterhaching
2023-10-20T19:33:57.66	not reported					Unterhaching
2023-10-24T00:43:56.32		0.96	WBRU.HLZ	2021-11-01T08:02:05	Unterhaching	Unterhaching
2023-10-24T14:26:23.05		0.94	WBRU.HLZ	2021-10-26T09:42:36	Unterhaching	Unterhaching
2023-10-24T14:40:56.08	not reported					Unterhaching
2023-10-24T16:28:00.07	not reported					Unterhaching
2023-10-27T01:56:06.43		0.71	WBRU.HLZ	2022-03-08T03:56:33	Oberhaching	Oberhaching
2023-11-19T20:14:15.84	not reported					
2023-11-20T04:31:21.07	not reported					
2023-11-19T20:14:17.50		0.73	SIEM.HL2	2021-10-22T23:21:44	Unterhaching	Unterhaching
2023-11-20T04:31:22.90		0.73	SIEM.HL2	2021-10-22T23:21:44	Unterhaching	Unterhaching
2023-11-29T08:28:43.50		0.73	SIEM.HL2	2021-10-22T23:21:44	Unterhaching	Unterhaching
2023-11-29T08:32:06.60		0.70	WBRU.HLN	2022-02-09T05:51:31	Unterhaching	Unterhaching

Trigger time (UTC)	SNR evaluation	Max correlation coefficient …	… on channel …	… and template from event …	Origin (suggested by template)	Event reported and located
				INSIDE		**LMU**
2023-11-29T11:38:40.10		0.73	SIEM.HL2	2021-10-22T23:21:44	Unterhaching	Unterhaching
2023-11-29T12:01:32.60		0.7	SIEM.HL2	2021-10-22T23:21:44	Unterhaching	Unterhaching
2023-12-15T03:39:28.29		0.77	WBRU.HLZ	2023-03-01T15:36:38	Oberhaching	not reported

4.2 OBSERVED SIGNAL TO NOISE RATIO (SNR)

Figure 6 gives a statistical overview of the SNR observed on the recordings of the five INSIDE stations. The figure shows the maximum SNR observed over the seismic signal associated with each event listed in Table 4. The statistics computed over the list of events are shown with boxplots, with whiskers ranging from minimum to maximum values in the distribution. The SNR values are evaluated in the 5 to 40 Hz frequency band that is used for event detection. The values are averaged over the three station channels, yielding a single observation for every pair of station – event.
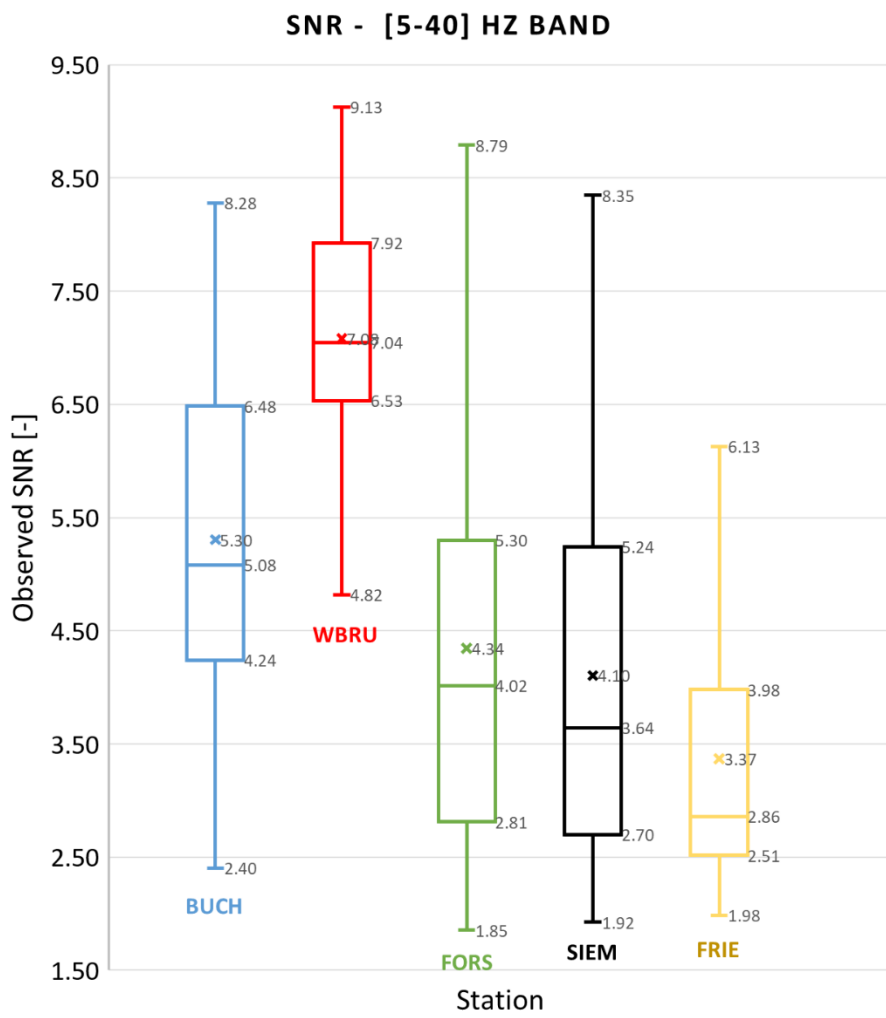
Figure 6: Statistical representation (boxplot) for every event listed in Table 4 of SNR values measured in the 5-40 Hz frequency band. This band is selected for event detection. Single SNR values are obtained as an average of the SNR measured on every station channel. The middle horizontal line indicates the median and the cross indicates the mean value. The whiskers show the upper and lower quartiles.

Figure 6 highlights overall higher SNR values for the WBRU seismic station, which can be attributed to its location to the southeast of the network, in closer proximity to the Unterhaching / Oberhaching sites. These measurements underscore that, based on the events detected during the project, station WBRU offers the most valuable contribution to the detection over the INSIDE network, contributing also significantly to the picking of onset times due to the high SNR.

For local seismic monitoring, we assume that a SNR of 3 is necessary to enable a suitable evaluation of onset times on the seismic recordings. The borehole station SIEM gives contrasted results, in the same way as FORS. The mean and median SNR is higher than 3, but the boxplot shows a strong variability within the series of values. A precise evaluation of the contribution of the borehole station

and of the FORS station, which evidenced low noise conditions, will be the subject of a separate report. FRIE generally provides lowest SNR values, and the recordings yield poor arrival time measurements (mean and median SNR below 3).

The SNR observed at a given station depends, among others, on the distance to the seismic source. As, the detected events are concentrated in the south-east/east of the network, the statistical distributions are necessarily influenced. Hence, the measurements presented for each station in Figure 6 are tied to the observations made during the monitoring period and do not represent absolute sensitivities. In this context, a normalization of the SNR to the source-to-receiver distance is carried out in a subsequent report to compare the capabilities of the measurement stations.

4.3 SIGNAL ON "UNCONVENTIONAL" MONITORING STATIONS

Here, we refer to as "unconventional" monitoring stations those that differ from a typical surface station equipped with a broadband geophone. This includes the DAS-station in Buchenhain, the mini-array in Siemens Park and the borehole station in Siemensallee. An assessment of the pros and cons of these various instruments and configurations for local (micro-) seismic monitoring is necessary. We use the timing and location information of the events listed in Table 4 to compare the monitoring instruments and recording configurations deployed during the project. By looking into the mini-array and DAS data at these specific dates, we aim to:

- Assess the strength of seismic signals on the recordings of the DAS station and the mini-array,
- Evaluate the feasibility of utilizing these signals for source characterization. This involves locating the event (at least, describing the back azimuth) and assessing the magnitude (local and / or moment magnitude).

In Table 5, we distinguish for all events detected during the period of operation of the Buchenhain DAS station and the mini-array

- Events characterized by a signal on the DAS channels or the mini-array stations that is too weak or overshadowed by significant background noise, preventing the identification and processing of the signal for event description (white background).
- Events where the signal of interest is identified on distinct traces, but the observed signal-to-noise ratio hinders the processing (light green background).
- Events for which the signals, in view of the observed signal-to-noise ratio, make it possible to consider processing the recordings with the aim of characterizing the event (dark green background).

A more comprehensive comparison of seismic signal detectability and monitoring outcomes from these "unconventional" monitoring stations will be detailed in a subsequent report, with a focus on the events highlighted in Table 5.

Table 5: Qualitative assessment of seismic signals across various instrument types. For each event in Table 4, columns 2 shows if the event location is possible from the recordings of the seismometer network (dark green background) and column 3 indicates the origin of the events based on the template analysis. The table details then if the seismic signals observed on the DAS measurement points (in Buchenhain) or on the stations of the mini-array (Siemens Park) at these specific dates allow the further processing of the signals, in view of the event description.

	Further processing is possible (e.g. location)
	The signal is observed on channels / stations

Trigger time (UTC)	INSIDE seismometer network		Visible on	
	Signal assessment	**Origin (from templates)**	**DAS - BUCH**	**SIEM - mini-array**
2021-03-05T21:56:23.24		Oberhaching		
2021-03-30T00:34:54.28		Oberhaching		
2021-06-04T14:55:57.89		Other		
2021-06-08T05:42:51.00		Oberhaching		
2021-06-18T16:40:02.38		Oberhaching		
2021-06-18T16:43:58.10		Oberhaching		
2021-06-18T17:01:45.22		Oberhaching		
2021-06-18T19:27:44.00		Oberhaching		
2021-06-19T01:40:37.00		Oberhaching		
2021-06-19T02:13:32.11		Oberhaching	**START**	
2021-10-22T17:55:02.50		Unterhaching		
2021-10-22T23:21:43.00		Unterhaching		
2021-10-23T03:05:39.60		Unterhaching		
2021-10-23T04:52:44.50		Unterhaching		
2021-10-23T18:51:16.60		Unterhaching		
2021-10-26T09:42:38.00		Unterhaching		
2021-10-28T21:49:11.80		Unterhaching		
2021-11-01T08:02:07.50		Unterhaching		
2021-12-03T15:24:11.50		Oberhaching		

Trigger time (UTC)	INSIDE seismometer network		Visible on	
	Signal assessment	Origin (from templates)	DAS - BUCH	SIEM - mini-array
2021-12-03T21:52:56.10		Unterhaching		
2022-01-18T23:52:53.50		Unterhaching		
2022-02-09T05:51:32.00		Unterhaching	No data	
2022-02-09T11:48:55.00		Unterhaching	No data	
2022-03-01T05:25:33.00		Unterhaching	No data	
2022-03-06T03:58:59.50		Oberhaching	No data	
2022-03-08T03:56:34.00		Oberhaching	No data	
2022-03-08T04:28:26.00		Oberhaching	No data	
2022-03-08T04:30:55.30		Oberhaching	No data	
2022-04-16T11:39:19.00		Oberhaching		
2022-04-23T12:10:58.00		Unterhaching		
2022-04-23T20:29:10.20		Unterhaching		
2022-05-21T22:24:11.50		Oberhaching		
2022-05-21T23:14:04.00		Oberhaching		
2022-05-21T23:48:19.50		Oberhaching		START
2022-05-26T20:51:30.00		Oberhaching		
2022-08-11T10:15:02.50		Oberhaching		
2022-09-07T00:56:43.00		Unterhaching		
2022-09-07T02:07:55.00		Unterhaching		
2022-09-25T14:48:05.50		Oberhaching		
2022-12-05T22:35:52.20		Unterhaching		
2022-12-09T03:21:41.50		Oberhaching		
2022-12-27T03:49:29.00		Oberhaching		
2023-01-15T21:08:04.00		Pullach (Th3)		
2023-02-25T15:35:00.20		Oberhaching		
2023-03-01T15:36:38.80		Oberhaching		

Trigger time (UTC)	INSIDE seismometer network		Visible on	
	Signal assessment	Origin (from templates)	DAS - BUCH	SIEM - mini-array
2023-03-06T08:52:15.30		Oberhaching		
2023-03-09T01:21:34.00		Oberhaching		
2023-04-22T23:06:43.10		Pullach (Th3)	No data	
2023-05-06T06:43:56.50		Oberhaching	No data	
2023-05-06T08:19:20.30		Oberhaching	No data	
2023-05-06T10:02:28.00		Oberhaching	No data	
2023-05-06T11:17:05.80		Oberhaching	No data	
2023-05-06T16:53:33.76		Oberhaching	No data	
2023-05-06T17:35:31.56		Oberhaching	No data	
2023-05-06T17:38:20.31		Oberhaching	No data	
2023-08-06T02:41:21.52		Oberhaching		
2023-08-06T02:51:48.98		Oberhaching		
2023-08-06T03:41:59.13		Oberhaching		
2023-08-06T03:43:01.05		Oberhaching		
2023-08-06T03:45:13.31		Oberhaching		
2023-08-06T03:50:34.72		Oberhaching		
2023-08-06T04:01:29.30		Oberhaching		
2023-08-06T04:25:01.66		Oberhaching		
2023-08-06T04:25:05.00		Oberhaching		
2023-08-06T04:36:51.28		Oberhaching		
2023-08-06T04:58:06.84		Oberhaching		
2023-08-06T04:58:39.66		Oberhaching		
2023-08-06T05:47:18.40		Oberhaching		
2023-10-17T03:09:50.70		Unterhaching		END
2023-10-24T00:43:56.32		Unterhaching		
2023-10-24T14:26:23.05		Unterhaching		

Trigger time (UTC)	INSIDE seismometer network		Visible on	
	Signal assessment	Origin (from templates)	DAS - BUCH	SIEM - mini-array
2023-10-27T01:56:06.43		Oberhaching		
2023-11-19T20:14:17.50		Unterhaching		
2023-11-20T04:31:22.90		Unterhaching		
2023-11-29T08:28:43.50		Unterhaching		
2023-11-29T08:32:06.60		Unterhaching		
2023-11-29T11:38:40.10		Unterhaching		
2023-11-29T12:01:32.60		Unterhaching		
2023-12-15T03:39:28.01		Oberhaching		

5 LOCATION OF SEISMIC EVENTS

5.1 ABSOLUTE LOCATION OF SEISMIC EVENTS

All seismic events listed in Table 4 are located following the procedure described in Section 10.2. The results presented in this paragraph are obtained using the "Model 1" of section 6, with a linear evolution of velocities with depth fitting closely the borehole data. In the report focusing on the development of velocity structures, we already showed that Model 1 results in a closer fit to the propagation times derived from the Pullach VSP carried out in PULL-TH3. This model will be further tested in the following.

As highlighted by Table 4, most of the detected events are associated with the Oberhaching (to the west) and Unterhaching (to the east) sites. The INSIDE network is not well suited for locating these events, as the two sites are positioned at the edge of the network. This results in a systematic bias in the inversion process. To compensate and be able to use the INSIDE recordings to assess the velocity structures, we use public data from the BayernNetz network (Department of Earth and Environmental Sciences, Geophysical Observatory, University of Munchen, 2001) to consolidate the recordings of the five INSIDE stations. Consequently, the epicenters shown in Figure 7 are derived from the onset times of P- and S-waves measured from the combined datasets. Locations are shown in the Gauss-Kruger 4 reference system. The event locations are listed in Table 6, where we provide further information about the associated errors and residuals. We also detail the epicenters reported by GOF/LMU, serving as a reference for comparison. As detailed in the legend, the color categories indicate the distance measured between the inverted event epicenters and the ones communicated by the Geophysical Observatory, when data are available simultaneously.

In Figure 7, the two events located near PULL TH3 are shown in white, as no reference data is available for the comparison. Three events are observed out of the main clusters of epicenters.

- The event near Baierbrunn (south-west) was observed by GOF/LMU and KIT. The distance between computed and communicated epicenters is larger than 2000 m. The hypocenter associated with the event is shallow, 558 m under mean see level. The associated waveforms, with strong signals simultaneously observed on all three channels, suggest an explosion, even if the origin of the event is not explained.
- We locate an event to the north of the western cluster associated with Oberhaching (origin time 2022-12-27T03:49:26.650 UTC, M_L -0.6). This event has not been observed by GOF. The signal is only faintly observed on four stations, which hinders its location.
- Another outlier is observed to the north of the western cluster associated with Oberhaching (origin time 2021-06-08T05:42:50.670 UTC). We compute an offset larger than 1.5 km with respect to the GOF measurement. This M_L -0.7 event is also only faintly observed over the network, which may explain inaccuracies in the event location.

Out of the previously mentioned outliers, offsets between computed and communicated epicenters remain largely below 1.0 km. These outliers are later removed from the catalog when comparing the velocity models (Section 6).
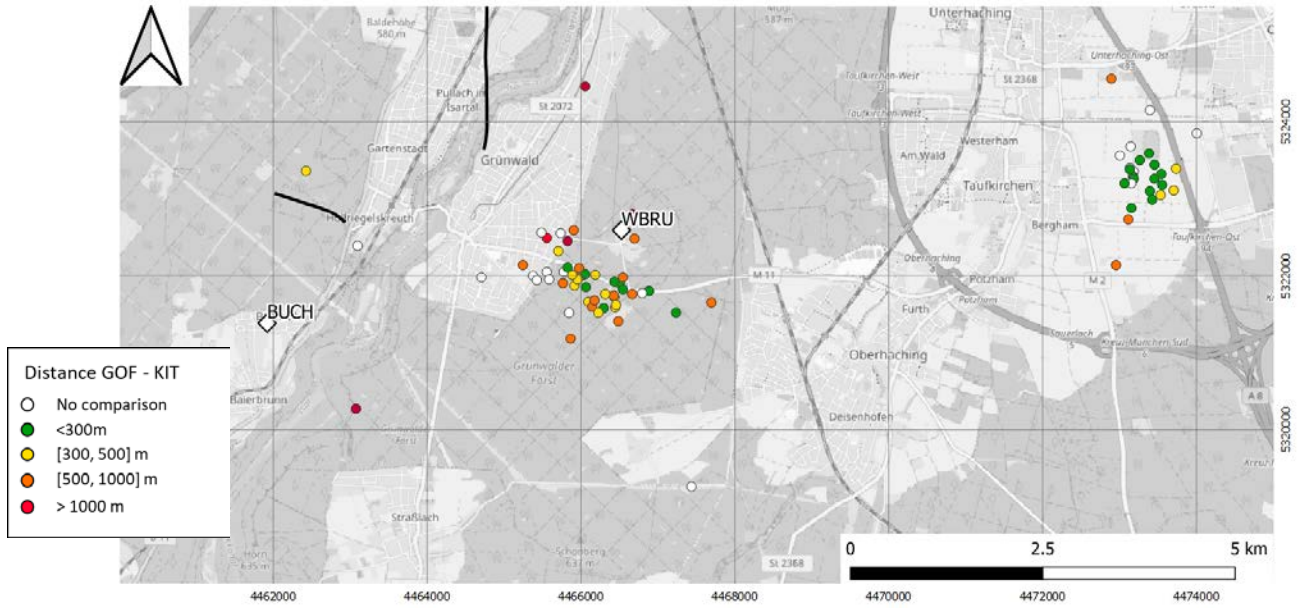
Figure 7: Map of epicenters computed for each event in Table 4. Seismic stations are denoted by green dots and the observations communicated by GOF are indicated by black dots. For each epicenter, we calculate the distance to the communicated location (background colors) when compatible data are available.

Figure 8 and Figure 9 provide a closer look the epicenters observed near the Oberhaching (Figure 8) and Unterhaching (Figure 9) sites. Overall, the epicenters measured in INSIDE are consistent with the communicated observations, with differences in locations globally smaller than 1km.
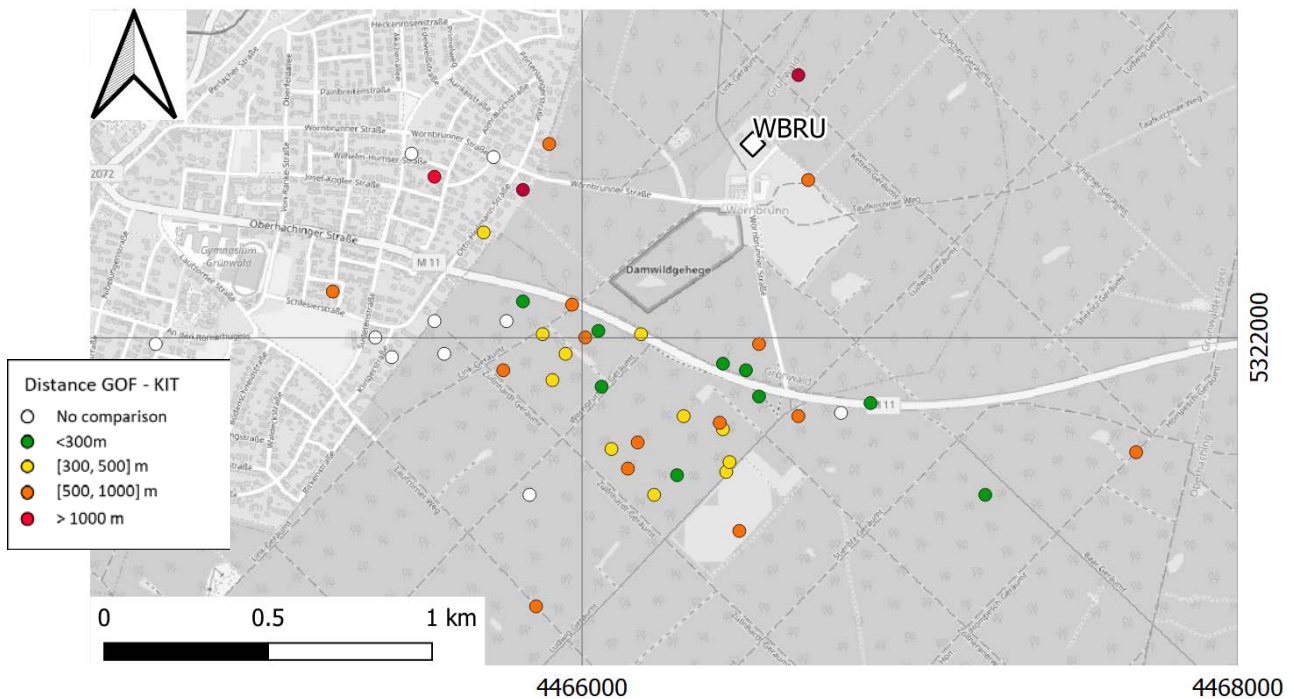
Figure 8: Map of computed epicenters, focusing on the events associated with the Oberhaching site (same legend as in Figure 7). The top panel shows the epicenters in comparison to the communicated measurements. The bottom panel shows the epicenters (Figure 7) with the associated origin times.
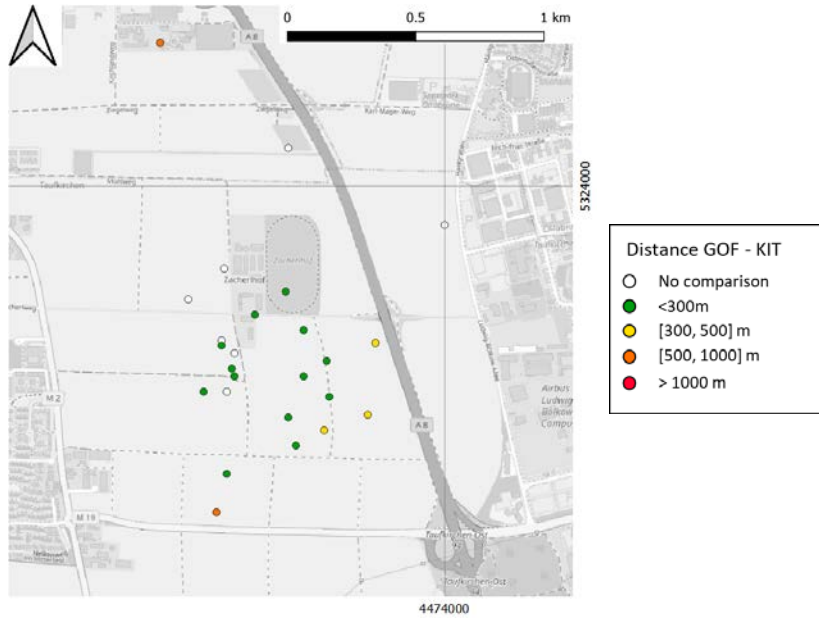
Figure 9: Map of epicenters, focusing on the events associated with the Unterhaching site (same legend as in Figure 7). The left panel shows the epicenters in comparison to the communicated measurements. The right panel shows the epicenters (Figure 7) with the associated origin times.

The depths of the hypocenters are shown in Figure 10 relative to an indicative reservoir depth. The uncertainties of the localization are also given in the form of error bars. The absolute localizations show that the events are localized in the reservoir or in the crystalline. Some events are localized in the near-surface sediment layers, particularly with larger uncertainties in the position determination. For these events, few arrival time measurements are available because they are only weakly detected by the seismometer network, which may lead to a possible bias in the localization.
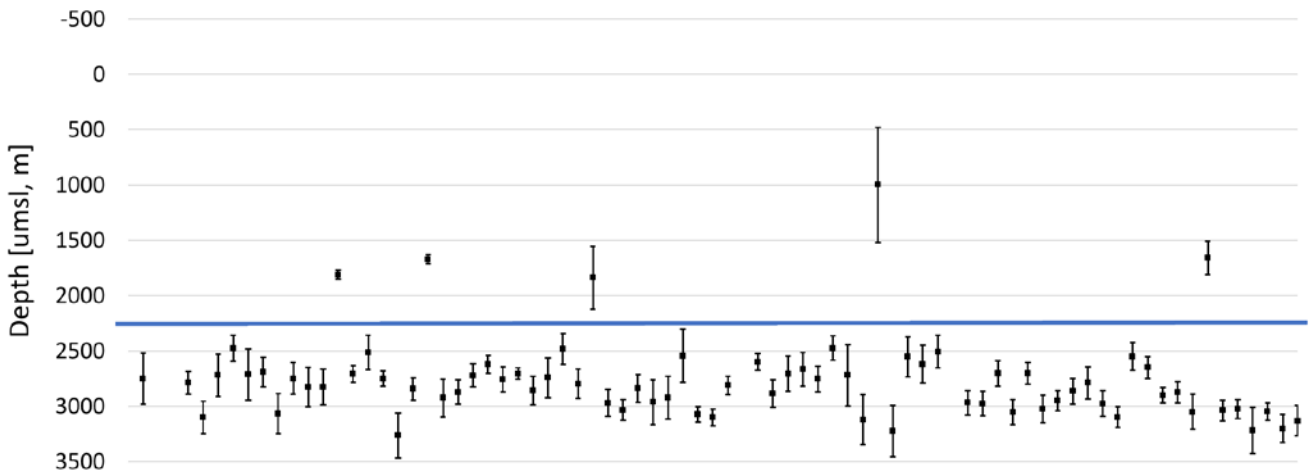
Figure 10: Depth of the absolute hypocenters of the 79 detected seismic events. The error bars correspond to the length of the semi-major axis of the 68% confidence ellipsoid and illustrate uncertainties in the location. The blue line is an indication of the depth of the reservoir.

.

Table 6: Catalog of events detected by the INSIDE seismometer network with locations, associated errors and magnitude estimation. The first column indicates the origin time, UTC referenced. Then, we give the event hypocenter in the Gauss-Kruger 4 coordinate system. The depth is referenced by respect to mean see level. Column 5 "Err 1" indicates the length of semi-major axis of 68% confidence ellipsoid. Column "Err 2" shows the maximal horizontal uncertainty, i.e. the length of the semi-minor axis of 68% confidence ellipsoid. "RMS residuals" shows the root-mean-square of residuals at maximum likelihood or expected epicenters. We estimate the local magnitude M_L and moment magnitude M_W from the location and station recordings. Finally, we compare the inverted results to the ones communicated by GOF (Tobias Megies, by personal communication).

KIT									LMU		
OT	Easting	Northing	Depth	Err 1	Err 2	RMS residuals	ML	MW	Easting	Northing	ML
[UTC]	[m, GK4]	[m, GK4]	[umsl, m]	[m]	[m]	[s]	[-]	[-]	[m, GK4]]	[m, GK4]	[-]
2021-03-05T21:56:23.128	4465630	5321830	3125	120	97	0.20	-0.1	0.0	4465980	5322050	0.0
2021-03-30T00:34:54.247	4465880	5322650	2816	231	186	0.08	-0.3	0.5	4465930	5322050	-0.3
2021-06-04T14:55:57.738	4463010	5320430	558	115	73	0.02	0.4	0.6	4461100	5318700	
2021-06-08T05:42:50.670	4466460	5324440	375	430	235	0.06	-0.7	0.5	4465770	5321650	-0.5
2021-06-18T16:40:02.180	4466060	5321690	2876	103	75	0.08	0.1	0.6	4466460	5321760	0.2
2021-06-18T16:43:57.191	4466120	5322150	3183	144	112	0.08	-0.1	0.6	4466360	5321710	-0.3
2021-06-18T17:01:45.058	4465840	5321930	2824	191	124	0.08	0.0	0.6	4466390	5321830	-0.1
2021-06-18T19:27:43.892	4465490	5322510	2454	120	95	0.11	-0.3	0.7	4465900	5321220	-0.3
2021-06-19T01:40:36.661	4465750	5322570	2790	232	153	0.06	-0.6	0.6	4466800	5320950	-1.0
2021-06-19T02:13:31.698	4466230	5321610	2885	133	106	0.12	-0.5	0.5	4466320	5321940	-0.5
2021-10-22T17:55:00.935	4473080	5323310	3225	180	136	0.10	0.5	0.6	4473100	5323390	0.4
2021-10-22T23:21:40.367	4473050	5323400	2825	142	86	0.08	0.0	0.6			
2021-10-23T03:05:35.857	4473110	5323530	2900	176	103	0.09	0.2	0.6	4473000	5323400	0.3
2021-10-23T04:52:41.428	4472990	5323190	2924	160	103	0.11	0.0	0.6			
2021-10-23T18:51:14.082	4472880	5324450	2800	43	34	0.09	0.7	0.8	4472590	5324110	0.7
2021-10-26T09:42:34.333	4473100	5323280	2825	75	43	0.10	0.5	0.6	4472970	5323420	0.6
2021-10-28T21:49:08.042	4473050	5323640	2725	155	119	0.06	-0.1	0.6			
2021-11-01T08:02:03.934	4473050	5323390	2850	71	39	0.09	0.6	0.7	4473090	5323340	0.6
2021-12-03T15:24:10.818	4466540	5321850	3391	200	161	0.10	-0.2	0.5	4466440	5322320	-0.2
2021-12-03T21:52:53.315	4473320	5323630	2900	99	52	0.09	0.3	0.4	4473230	5323680	0.4

KIT									LMU		
2022-01-18T23:52:50.846	4473610	5323930	2352	40	21	0.13	-0.1	0.5			
2022-02-09T05:51:29.056	4473610	5323520	2959	170	50	0.10	1.2	0.6	4473505	5323680	1.4
2022-02-09T11:48:52.196	4473260	5323320	2875	110	69	0.07	0.5	0.6	4473510	5323510	0.6
2022-03-01T05:25:30.971	4473940	5323800	2850	105	59	0.07	-0.2	0.5			
2022-03-06T03:58:58.040	4465170	5322170	2650	79	48	0.12	-0.5	0.6	4466080	5322110	-0.5
2022-03-08T03:56:32.669	4466470	5321950	2793	112	90	0.10	-0.5	0.5	4466420	5322020	-0.4
2022-03-08T04:28:24.469	4466370	5321810	2826	51	41	0.11	0.0	0.5	4466600	5322060	0.1
2022-03-08T04:30:53.798	4466720	5322630	2844	130	103	0.10	-0.3	0.5	4465980	5322280	-0.3
2022-04-16T11:39:17.842	4466710	5322960	2699	180	112	0.08	-0.3	0.6	4465700	5320500	-0.3
2022-04-23T12:10:55.243	4473200	5322820	2564	140	55	0.07	0.3	0.6	4472990	5322800	0.5
2022-04-23T20:29:07.895	4472830	5322110	2862	132	91	0.08	0.3	0.6	4472990	5322760	0.7
2022-05-21T22:24:10.619	4465450	5322340	2027	282	215	0.07	-0.6	0.6			
2022-05-21T23:14:02.820	4466600	5321910	3099	122	98	0.10	-0.1	0.6	4466320	5321690	-0.1
2022-05-21T23:48:18.186	4466350	5322080	3100	95	75	0.10	-0.5	0.6	4466240	5322010	-0.6
2022-05-26T20:51:28.815	4465730	5322230	2894	126	83	0.11	-0.3	0.5	4466070	5322200	-0.2
2022-08-11T10:15:01.338	4465610	5322350	3024	201	135	0.09	0.0	0.5	4466100	5322230	0.0
2022-09-07T00:56:39.700	4473010	5323450	3007	193	119	0.10	0.1	0.6			
2022-09-07T02:07:50.996	4472910	5323480	2730	239	100	0.07	-0.3	0.5			
2022-09-25T14:48:04.260	4465960	5322050	3172	69	53	0.14	0.8	1.0	4465850	5322340	0.8
2022-12-05T22:35:50.469	4466790	5321810	3127	76	62	0.12	-0.6	0.4			
2022-12-09T03:21:40.631	4467720	5321720	2946	85	69	0.11	-0.3	0.6	4467170	5322050	-0.7
2022-12-27T03:49:26.645	4467420	5320330	4510	240	190	0.22	-0.6	0.6			
2023-01-15T21:08:02.991	4463120	5322350	2774	76	45	0.10	-0.4	-0.3			
2023-02-25T15:34:58.755	4466820	5321880	3012	125	100	0.08	0.2	0.6	4467050	5321800	0.4
2023-03-01T15:36:37.155	4467190	5321580	2790	161	129	0.10	0.1	0.7	4467310	5321650	0.1
2023-03-06T08:52:13.789	4466460	5322080	2725	152	116	0.09	0.0	0.7	4467230	5321790	0.1
2023-03-09T01:21:32.644	4465510	5322120	2825	115	75	0.12	-0.2	0.5			

KIT									LMU		
2023-04-22T23:06:42.037	4462370	5323350	2633	111	60	0.12	-0.4	0.4	4462449	5323019	-0.2
2023-05-06T06:43:55.604	4465370	5322000	2851	277	145	0.10	-0.2	0.6			
2023-05-06T08:19:19.249	4465630	5322150	3170	226	144	0.10	-0.1	0.6			
2023-05-06T10:02:27.415	4464710	5321960	1224	520	420	0.08	-0.5	0.6			
2023-05-06T11:17:04.740	4465700	5321580	3350	231	120	0.08	-0.2	0.7			
2023-05-06T16:53:32.768	4465590	5321990	2661	180	158	0.08	-0.1	0.7			
2023-05-06T17:35:30.501	4465340	5322040	2676	170	126	0.08	-0.4	0.7			
2023-05-06T17:38:18.894	4465670	5322630	2497	150	135	0.07	-0.3	0.5			
2023-07-18T20:56:24.390	4471500	5326000	150	150	122	0.09	-0.2	0.2			
2023-08-06T02:41:20.347	4466500	5321450	3110	110	84	0.12	-0.3	0.4	4466630	5321910	-0.4
2023-08-06T02:51:47.874	4466430	5321820	3151	111	87	0.08	0.2	0.4	4466750	5321900	0.3
2023-08-06T03:41:58.064	4465830	5321880	2933	115	89	0.13	-0.3	0.6	4466460	5321780	-0.2
2023-08-06T03:42:59.948	4466250	5321670	3133	112	79	0.12	-0.2	0.6	4466310	5321830	-0.1
2023-08-06T03:45:12.283	4465920	5322030	2775	97	63	0.10	-0.3	0.6	4466300	5321790	-0.2
2023-08-06T03:50:33.596	4466030	5321990	3132	125	119	0.10	-0.3	0.6	4466260	5321840	-0.6
2023-08-06T04:01:28.191	4466460	5321690	3083	93	62	0.11	-0.1	0.6	4466630	5321920	0
2023-08-06T04:25:00.528	4466390	5321700	2975	117	93	0.12	-0.4	0.4	4466760	5321840	-0.7
2023-08-06T04:25:03.979	4465950	5322100	2825	144	103	0.10			4466260	5321500	-0.9
2023-08-06T04:36:50.173	4466370	5321840	3087	116	84	0.08	0.2	0.4	4467206	5321785	0.1
2023-08-06T04:58:05.850	4465900	5322210	2599	93	69	0.07	-0.2	0.6	4466600	5321610	-0.5
2023-08-06T04:58:38.518	4466070	5321780	3176	127	95	0.10			4466790	5321920	-0.5
2023-08-06T05:47:17.357	4466080	5321670	2679	101	71	0.09	-0.2	0.5	4466610	5321950	-0.3
2023-10-17T03:09:49.750	4473270	5323550	2925	71	52	0.10	0.6	0.6	4473510	5323380	0.7
2023-10-24T00:43:55.368	4472900	5323260	2916	99	62	0.08	0.2	0.6	4473100	5323310	0.7
2023-10-24T14:26:22.168	4472940	5322710	3088	160	118	0.10	0.6	0.6	4473060	5323370	0.7
2023-10-27T01:56:06.513	4465660	5321110	1371	150	160	0.05	-0.8	0.4	4466110	5321880	-0.2
2023-11-19T20:14:15.719	4473260	5323110	3192	93	62	0.11	0.5	0.5	4473450	5323350	0.6

KIT									LMU		
2023-11-20T04:31:20.976	4473190	5323190	3050	84	52	0.11	1.2	1.2	4473470	5323190	1.4
2023-11-29T08:28:41.497	4473380	5323260	3340	208	114	0.10	0.5	0.7	4473610	5323460	0.9
2023-11-29T08:32:04.550	4473600	5323210	3067	79	50	0.11	1.1	1.2	4473500	5323390	1.3
2023-11-29T11:38:38.194	4473300	5323030	3425	125	63	0.11	1.6	1.0	4473516	5323457	1.8
2023-11-29T12:01:30.679	4473350	5323470	3250	135	78	0.09	1.4	1.5	4473660	5323410	1.6

Figure 11 graphically illustrates the error and residual values listed in columns 5 to 7 of Table 6. The boxplots illustrate the statistical distribution obtained from the 79 located events. From left to right, we consider different indicators:

- the length of semi-major axis of 68% confidence ellipsoid,
- the lengths of semi-minor axis of 68% confidence ellipsoid,
- the root-mean-square (RMS) values of residuals at maximum likelihood,
- the station residuals.
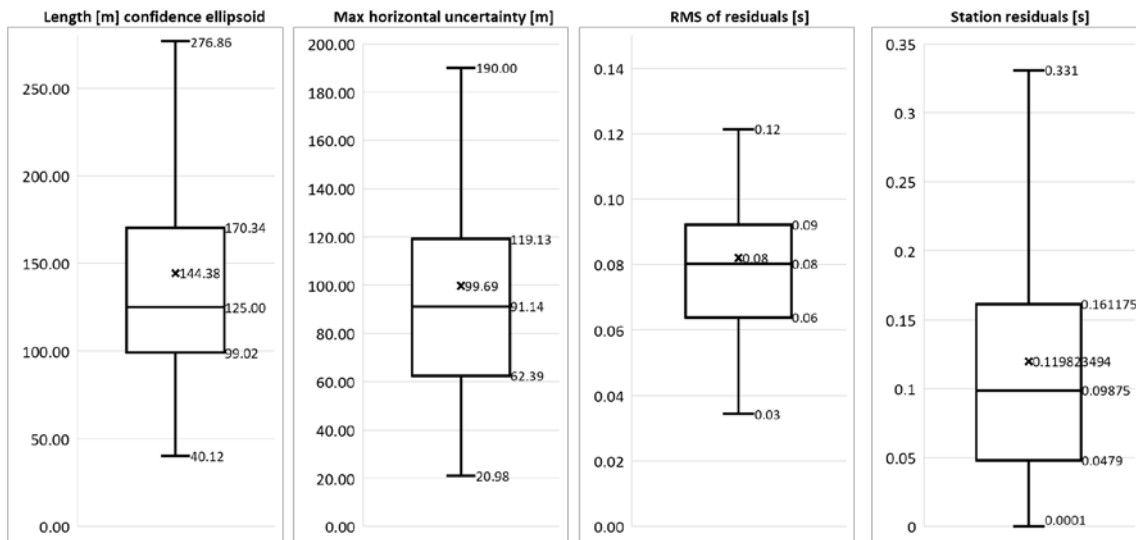
Figure 11: Statistical representation (boxplot) of the residuals and errors listed in Table 6. From left to right, the boxplot includes the distribution of lengths of semi-major-axis of 68% confidence ellipsoid, then the distribution of lengths of semi-minor axis of 68% confidence ellipsoid, then the root-mean-square (RMS) values of residuals at maximum likelihood and finally the station residuals. The whiskers extend to the upper and lower quartile, the cross shows the mean and the line the median of the series.

Figure 12 shows local magnitudes listed in Table 6 and compares the measured (X-axis) to the communicated values (Y-axis). The figure covers all events for which compatible data is available. The shaded region indicates a 1-to-1 ratio in observed and communicated local magnitudes with a ±0.1 margin.
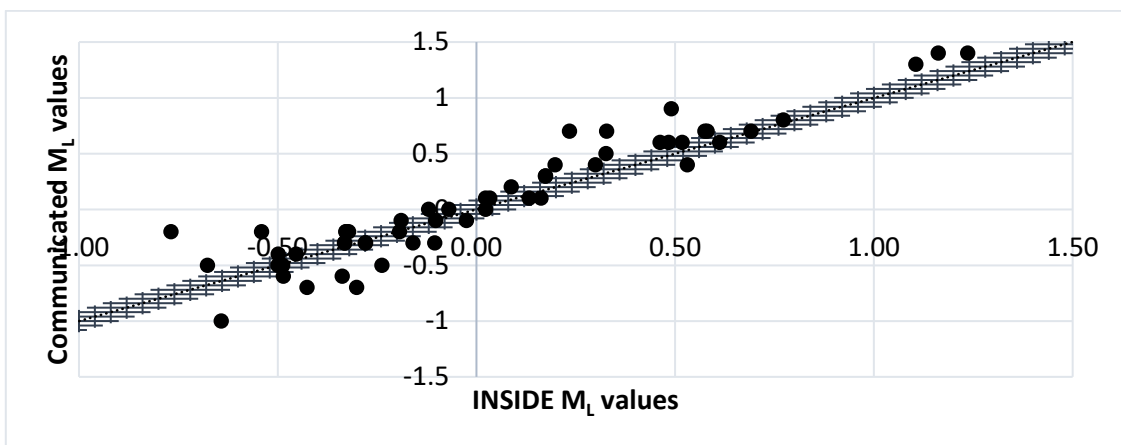
Figure 12: Scatter plot comparing the local magnitudes measured by KIT to those communicated by GOF (see Table 6). The comparison covers all events with compatible data. The shaded region represents a ±0.1 margin of error.

5.2 RELATIVE LOCATION OF SEISMIC EVENTS

The implementation of relative location methods allows locating the events relatively to each other. This additional processing step contributes to decrease uncertainties and inaccuracies between events. However, the cloud of events can also be simply shifted.

We calculate relative locations for all events listed in Table 6 following the procedure detailed in Sect. 10.3. Three clusters are identified (Pullach, Unterhaching and Oberhaching) with the characteristics detailed in Table 7.

Table 7: Barycenter of identified clusters during event relocation

Name	Number of events	Barycenter		
		X [km]	Y [km]	Z [km]
Pullach	2	4462.755	5322.875	2.538
Oberhaching	47	4466.110	5321.933	2.732
Unterhaching	26	4473.309	5323.330	2.79

The results obtained using the software package GrowClust3D (Trugman et al., 2023) are detailed in Table 8 and shown in Figure 13. The algorithm relocated 75 events among 79, discarding the outliers mentioned in Sect. 5.1, i.e. events lying strongly outside the main clusters of Table 7.
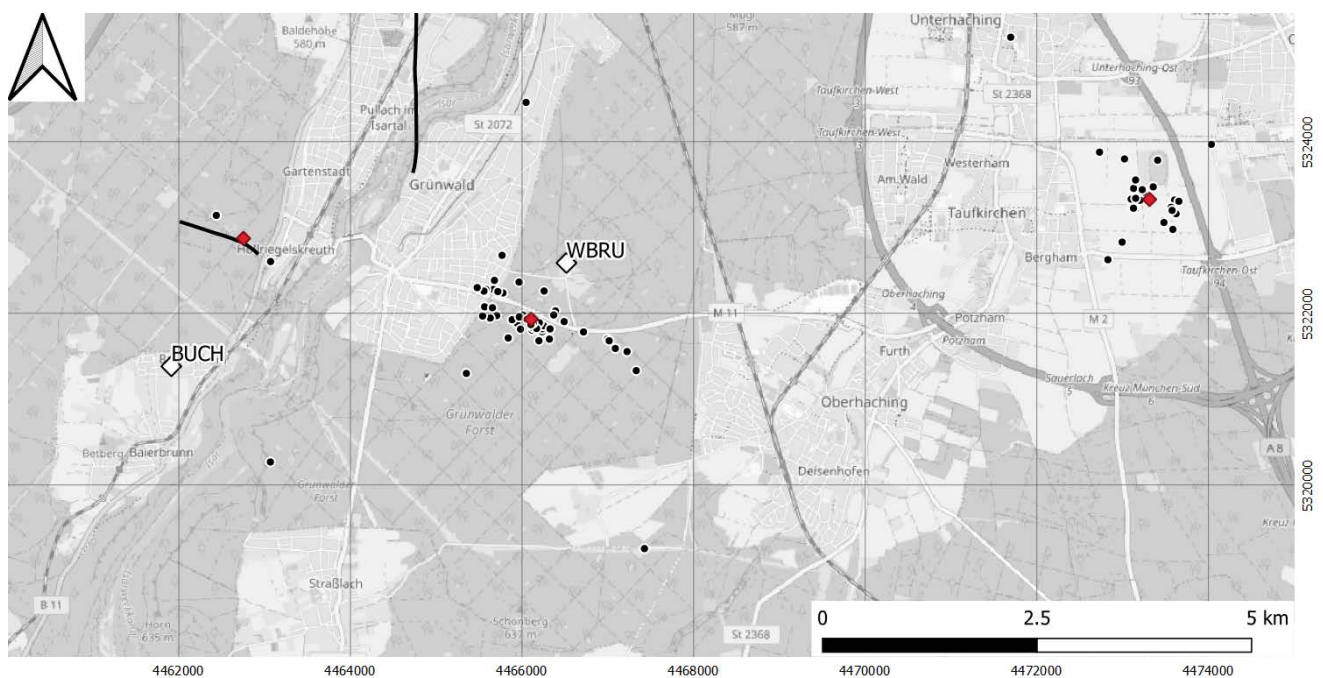
Figure 13: Map of the epicenters for all relative locations including the barycenter of identified clusters (red diamond).

After relative location of the seismic events, the clusters are overall more compact around the locations listed in Table 7. We observe a slight decrease of about 100 m of the average distance between computed and communicated epicenters (see Figure 14), suggesting that the relocated epicenters are more consistent with the communicated measurements.
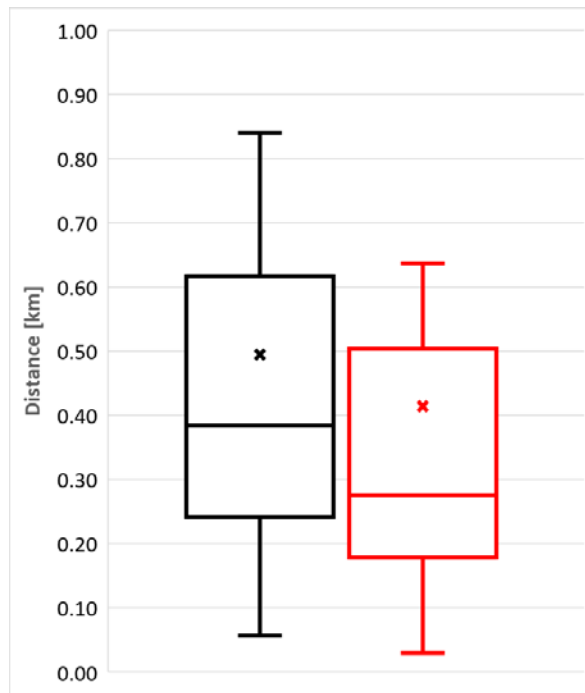
Figure 14: Statistical representation of the distances between communicated and computed epicenters, before (black) and after (red) relocation of the catalog.

We observe also that the relative location of seismic events provides more consistent hypocenter depths (Figure 15).
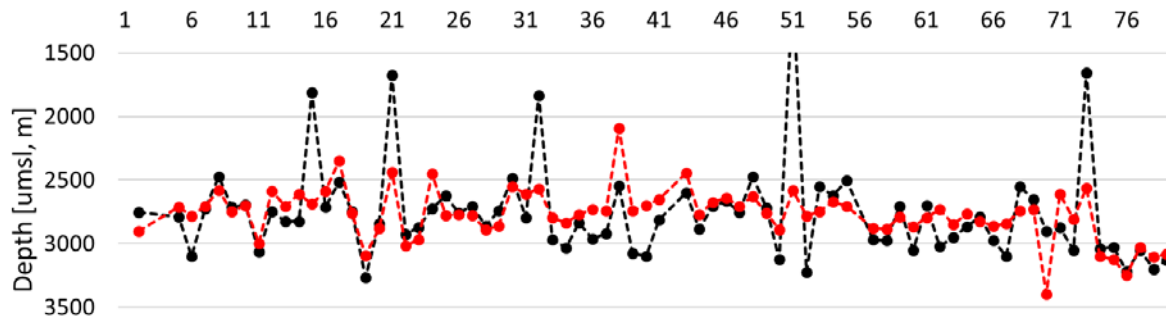
Figure 15: Comparison of hypocenter depth before (black) and after (red) relocation of the catalog. The hypocenter depth is shown in each case as a function of the event number (classified by date, from oldest to most recent)

Table 8: Catalog of relocated events and communicated epicenters

KIT, after relocation						LMU		
OT [UTC]	Easting [m, GK4]	Northing [m, GK4]	Depth [umsl, m]	ML [-]	MW [-]	Easting [m, GK4]]	Northing [m, GK4]	ML [-]
2021-03-05T21:56:23.231	4466261	5322263	1972	-0.1	0.0	4465980	5322050	0.0
2021-03-30T00:34:54.244	4465670	5322281	2901	-0.3	0.5	4465930	5322050	-0.3
2021-06-04T14:55:57.859	4463070	5320270	525	0.4	0.6	4461100	5318700	
2021-06-08T05:42:50.693	4466050	5324460	274	-0.7	0.5	4465770	5321650	-0.5
2021-06-18T16:40:02.269	4465943	5321890	2711	0.1	0.6	4466460	5321760	0.2
2021-06-18T16:43:57.276	4466015	5321982	2784	-0.1	0.6	4466360	5321710	-0.3
2021-06-18T17:01:45.129	4465888	5321928	2703	0.0	0.6	4466390	5321830	-0.1
2021-06-18T19:27:44.018	4465770	5322678	2580	-0.3	0.7	4465900	5321220	-0.3
2021-06-19T01:40:36.678	4465971	5321960	2748	-0.6	0.6	4466800	5320950	-1.0
2021-06-19T02:13:31.803	4466119	5321807	2701	-0.5	0.5	4466320	5321940	-0.5
2021-10-22T17:55:01.038	4473144	5323219	2995	0.5	0.6	4473100	5323390	0.4
2021-10-22T23:21:40.446	4473124	5323458	2588	0.0	0.6			
2021-10-23T03:05:35.940	4473238	5323415	2706	0.2	0.6	4473000	5323400	0.3
2021-10-23T04:52:41.504	4473224	5323444	2613	0.0	0.6			
2021-10-23T18:51:14.116	4472726	5323881	2690	0.7	0.8	4472590	5324110	0.7
2021-10-26T09:42:34.464	4473095	5323333	2589	0.5	0.6	4472970	5323420	0.6
2021-10-28T21:49:08.113	4473146	5323556	2351	-0.1	0.6			
2021-11-01T08:02:04.032	4473120	5323232	2758	0.6	0.7	4473090	5323340	0.6
2021-12-03T15:24:10.863	4467335	5321335	3094	-0.2	0.5	4466440	5322320	-0.2
2021-12-03T21:52:53.406	4473352	5323476	2876	0.3	0.4	4473230	5323680	0.4
2022-01-18T23:52:50.930	4473403	5323786	2440	-0.1	0.5			
2022-02-09T05:51:29.151	4473601	5323284	3018	1.2	0.6	4473505	5323680	1.4
2022-02-09T11:48:52.232	4473601	5323323	2966	0.5	0.6	4473510	5323510	0.6

KIT, after relocation						LMU		
OT [UTC]	Easting [m, GK4]	Northing [m, GK4]	Depth [umsl, m]	ML [-]	MW [-]	Easting [m, GK4]]	Northing [m, GK4]	ML [-]
2022-03-01T05:25:31.066	4474029	5323972	2448	-0.2	0.5			
2022-03-06T03:58:58.122	4465582	5322281	2780	-0.5	0.6	4466080	5322110	-0.5
2022-03-08T03:56:32.748	4466393	5322031	2770	-0.5	0.5	4466420	5322020	-0.4
2022-03-08T04:28:24.616	4466373	5321983	2779	0.0	0.5	4466600	5322060	0.1
2022-03-08T04:30:53.849	4466494	5321906	2890	-0.3	0.5	4465980	5322280	-0.3
2022-04-16T11:39:17.860	4465968	5322367	2861	-0.3	0.6	4465700	5320500	-0.3
2022-04-23T12:10:55.379	4472989	5322832	2548	0.3	0.6	4472990	5322800	0.5
2022-04-23T20:29:07.998	4472824	5322627	2612	0.3	0.6	4472990	5322760	0.7
2022-05-21T22:24:10.618	4465842	5321715	2569	-0.6	0.6			
2022-05-21T23:14:02.931	4466186	5321812	2795	-0.1	0.6	4466320	5321690	-0.1
2022-05-21T23:48:18.272	4466131	5321837	2838	-0.5	0.6	4466240	5322010	-0.6
2022-05-26T20:51:28.927	4465780	5322240	2773	-0.3	0.5	4466070	5322200	-0.2
2022-08-11T10:15:01.418	4465721	5322256	2730	0.0	0.5	4466100	5322230	0.0
2022-09-07T00:56:39.795	4473197	5323320	2742	0.1	0.6			
2022-09-07T02:07:51.074	4473017	5323801	2091	-0.3	0.5			
2022-09-25T14:48:04.406	4465681	5322386	2742	0.8	1.0	4465850	5322340	0.8
2022-12-05T22:35:50.639	4466720	5321785	2697	-0.6	0.4			
2022-12-09T03:21:40.743	4467228	5321557	2652	-0.3	0.6	4467170	5322050	-0.7
2022-12-27T03:49:26.650	4467430	5319260	2572	-0.6	0.6			
2023-01-15T21:08:03.050	4463071	5322606	2446	-0.4	-0.3			
2023-02-25T15:34:58.812	4467000	5321702	2773	0.2	0.6	4467050	5321800	0.4
2023-03-01T15:36:37.231	4467091	5321593	2677	0.1	0.7	4467310	5321650	0.1
2023-03-06T08:52:13.812	4467019	5321682	2641	0.0	0.7	4467230	5321790	0.1
2023-03-09T01:21:32.764	4465559	5322261	2703	-0.2	0.5			
2023-04-22T23:06:42.127	4462439	5323144	2630	-0.5	0.5	4462449	5323019	-0.2

KIT, after relocation						LMU		
OT [UTC]	Easting [m, GK4]	Northing [m, GK4]	Depth [umsl, m]	ML [-]	MW [-]	Easting [m, GK4]]	Northing [m, GK4]	ML [-]
2023-05-06T06:43:55.676	4465567	5322078	2759	-0.2	0.6			
2023-05-06T08:19:19.322	4465659	5322067	2893	-0.1	0.6			
2023-05-06T10:02:27.388	4465354	5321302	2580	-0.5	0.6			
2023-05-06T11:17:04.878	4465708	5321976	2785	-0.2	0.7			
2023-05-06T16:53:32.772	4465633	5321947	2745	-0.1	0.7			
2023-05-06T17:35:30.565	4465543	5321971	2670	-0.4	0.7			
2023-05-06T17:38:18.885	4465480	5322302	2704	-0.3	0.5			
2023-07-18T20:56:24.768	4471700	5325220	1500	-0.2	0.2			
2023-08-06T02:41:20.462	4466237	5321788	2877	-0.3	0.4	4466630	5321910	-0.4
2023-08-06T02:51:47.933	4466237	5321823	2887	0.2	0.4	4466750	5321900	0.3
2023-08-06T03:41:58.142	4466113	5321900	2789	-0.3	0.6	4466460	5321780	-0.2
2023-08-06T03:43:00.040	4466255	5321857	2865	-0.2	0.6	4466310	5321830	-0.1
2023-08-06T03:45:12.321	4466063	5321931	2794	-0.3	0.6	4466300	5321790	-0.2
2023-08-06T03:50:33.690	4466200	5321683	2729	-0.3	0.6	4466260	5321840	-0.6
2023-08-06T04:01:28.300	4466205	5321892	2846	-0.1	0.6	4466630	5321920	0.0
2023-08-06T04:25:00.619	4466322	5321702	2766	-0.4	0.4	4466760	5321840	-0.7
2023-08-06T04:25:04.017	4466330	5321821	2825			4466260	5321500	-0.9
2023-08-06T04:36:50.240	4466173	5321825	2859	0.2	0.4	4467206	5321785	0.1
2023-08-06T04:58:05.829	4466102	5321912	2844	-0.2	0.6	4466600	5321610	-0.5
2023-08-06T04:58:38.641	4466133	5321887	2741			4466790	5321920	-0.5
2023-08-06T05:47:17.410	4466106	5321871	2732	-0.2	0.5	4466610	5321950	-0.3
2023-10-17T03:09:49.770	4473581	5322980	3399	0.6	0.6	4473510	5323380	0.7
2023-10-24T00:43:55.423	4473147	5323343	2613	0.2	0.6	4473100	5323310	0.7
2023-10-24T14:26:22.256	4473122	5323227	2807	0.6	0.6	4473060	5323370	0.7
2023-10-27T01:56:06.449	4465985	5321817	2560	-0.8	0.4	4466110	5321880	-0.2

KIT, after relocation						LMU		
OT [UTC]	Easting [m, GK4]	Northing [m, GK4]	Depth [umsl, m]	ML [-]	MW [-]	Easting [m, GK4]]	Northing [m, GK4]	ML [-]
2023-11-19T20:14:15.824	4473471	5323083	3098	0.5	0.5	4473450	5323350	0.6
2023-11-20T04:31:21.041	4473477	5323061	3125	1.2	1.2	4473470	5323190	1.4
2023-11-29T08:28:41.619	4473619	5323163	3246	0.5	0.7	4473610	5323460	0.9
2023-11-29T08:32:04.677	4473561	5323237	3025	1.1	1.2	4473500	5323390	1.3
2023-11-29T11:38:38.296	4473651	5323308	3106	1.6	1.0	4473516	5323457	1.8
2023-11-29T12:01:30.756	4473572	5323202	3084	1.4	1.5	4473660	5323410	1.6

5.3 SPATIAL EVOLUTIONS OF THE SEISMICITY

To analyze the evolution of the seismic cloud over time, we plot the relocated locations, detailed in the previous table, with indication of the origin time in color (Figure 16 and Figure 18).

Figure 16: Map of all epicenters listed in Table 4 and that were detected across the study area during the INSIDE project. The color scale indicates number of days since first recorded event, on 2021-03-05T21:56:23.231 (UTC).

In parallel, we analyze the evolution of the seismic cloud as a function of the local magnitude. In Figure 17, the color scale indicates the observed local magnitude.
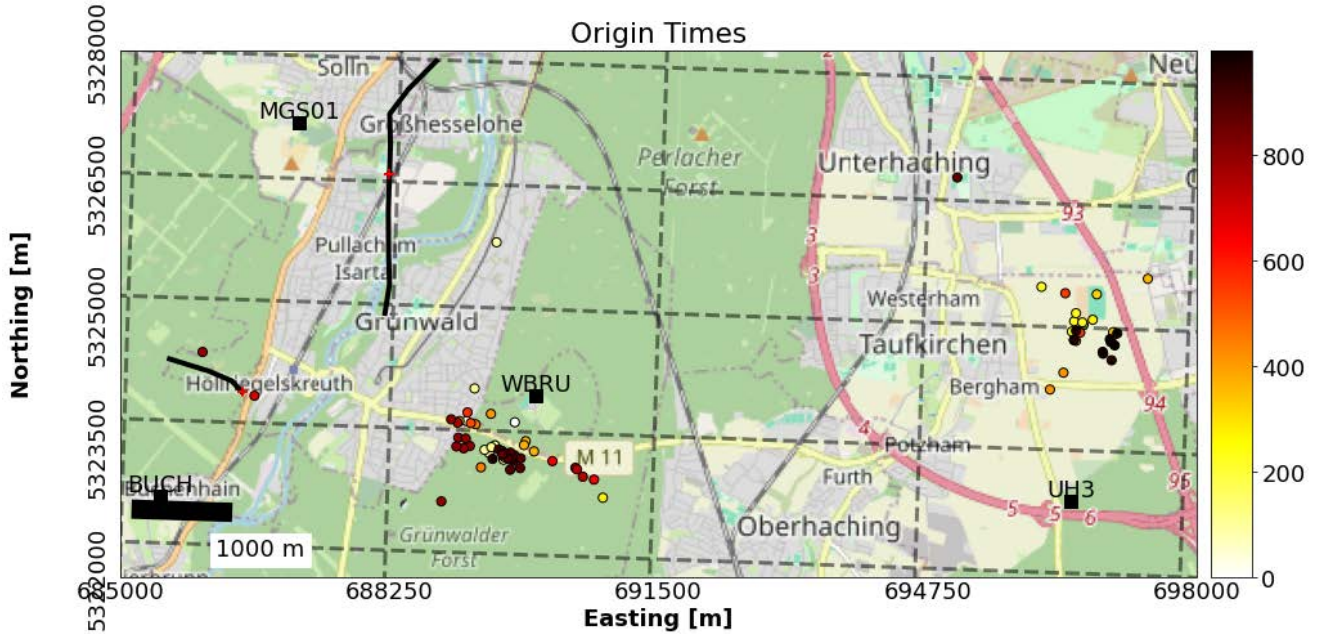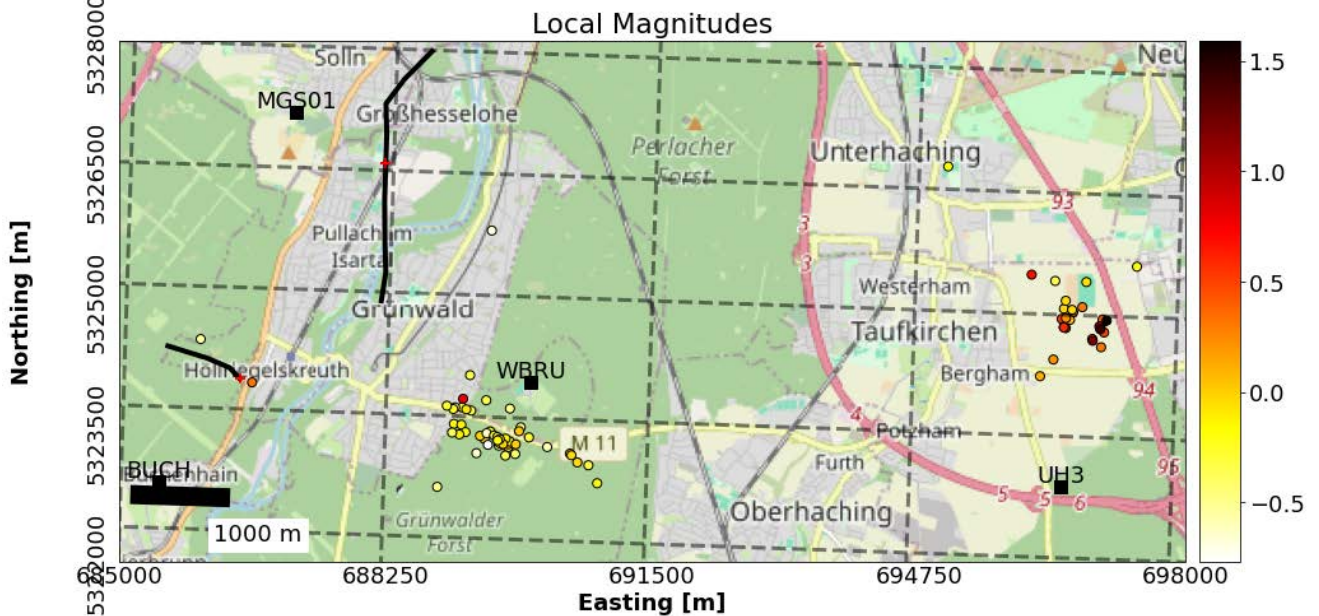

Figure 17: Map of all epicenters listed in Table 4 and that were detected across the study area during the INSIDE project. The color scale indicates the local magnitude computed for each event.
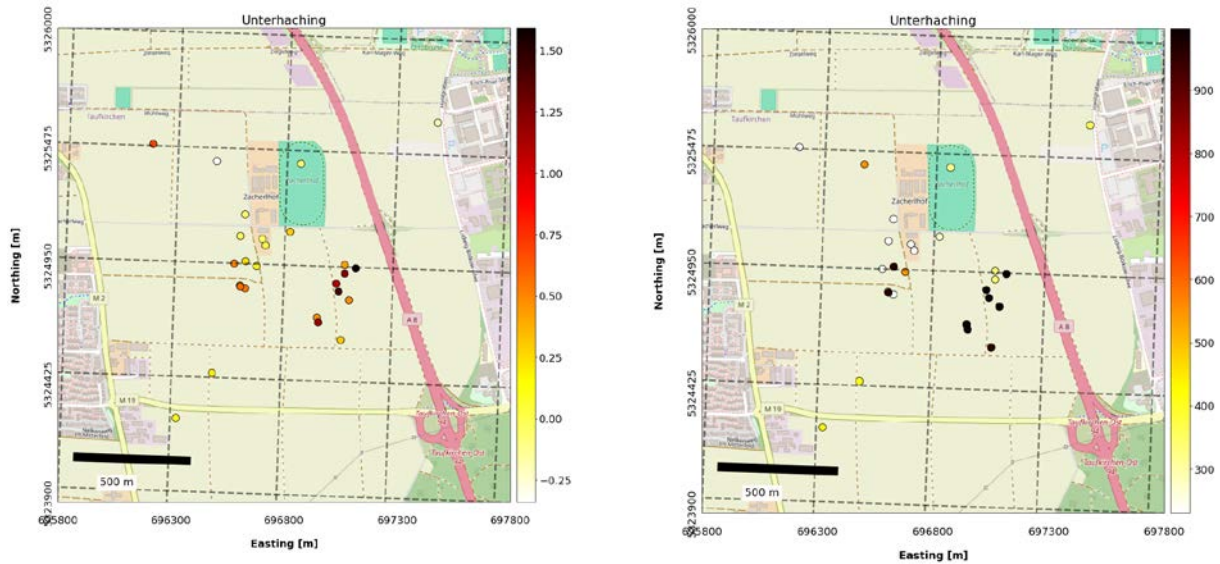
Figure 18: focus on Unterhaching with local magnitude (left) and origin time (right) for each event
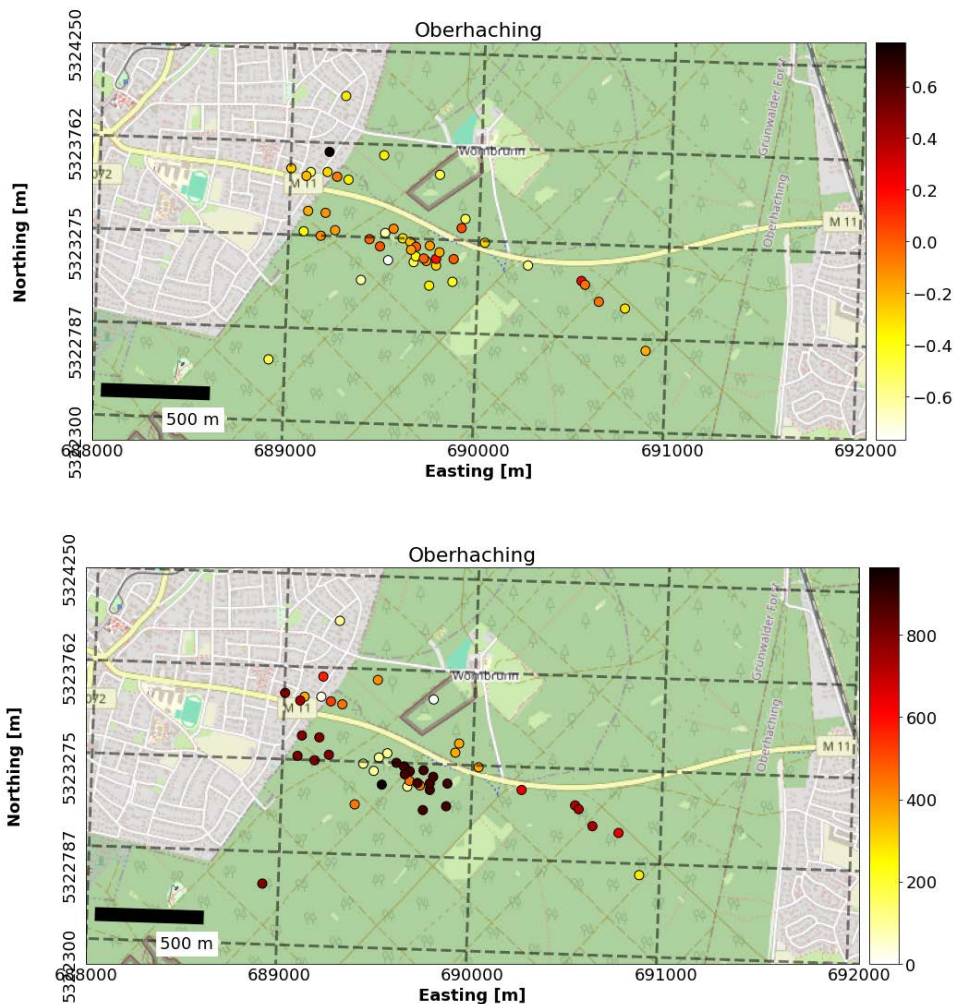
Figure 19: focus on Oberhaching with local magnitude (left) and origin time (right) for each event

Figure 16 to Figure 19 do not indicate a specific trend or temporal shift in the location of seismic events with time / magnitude. We observe, however, the clustering of seismic swarms, with nearby locations for events that occurred on August 2023 in Oberhaching (darker dots in Figure 19), for example.

6 COMPARISON OF VELOCITY MODELS

6.1 TESTED MODELS

Three different velocity structures covering the study area were constructed based on the geophysical data available within the project. They are based on different velocity profiles, using a linear or stepwise evolution of the velocity in the identified layers (see related report).

- **Model 1** is based on a closer fit to the logging and VSP results from Schäftlarnstraße and PULL-TH3. The model is based on a linear evolution of velocities with depth. The results listed in Table 6 are obtained using the associated velocity structure.
- **Model "cst"** is derived from Model 1. It is a blocky model for which we consider the velocities as constant in each layer.
- **Model "Erdwerk"** is based on a closer fit to the velocity blocs provided by Erdwerk GmbH. As model 1, it is based on a linear evolution of velocities with depth.

6.2 LOCATION RESULTS

Here, we evaluate the influence of these velocity structures on the inverted absolute locations. The objective is to validate the hypothesis made for the construction of Model 1, i.e. the linear evolution of velocities with depth (model 1 versus "cst") and assess the effect of both velocity profiles (model 1 versus "Erdwerk"). For this purpose, we analyze the results of the NLL hypocenter inversion to evaluate:

- The impact on event locations.
  - By comparing the obtained and communicated epicenters (Figure 20),
  - By analyzing the differences in inverted depth (Figure 20).
- The impact on inversion errors (Figure 21). We evaluate the size of the confidence ellipsoid by analyzing the length of its semi-major (left) and semi-minor (right) axis.
- The impact on inversion residuals (Figure 22).
  - We evaluate the difference between observed and expected (considering the inversion results) arrival times at stations.
  - Table 9 summarizes the total residuals measured for each phase and station, considering the three different structures.
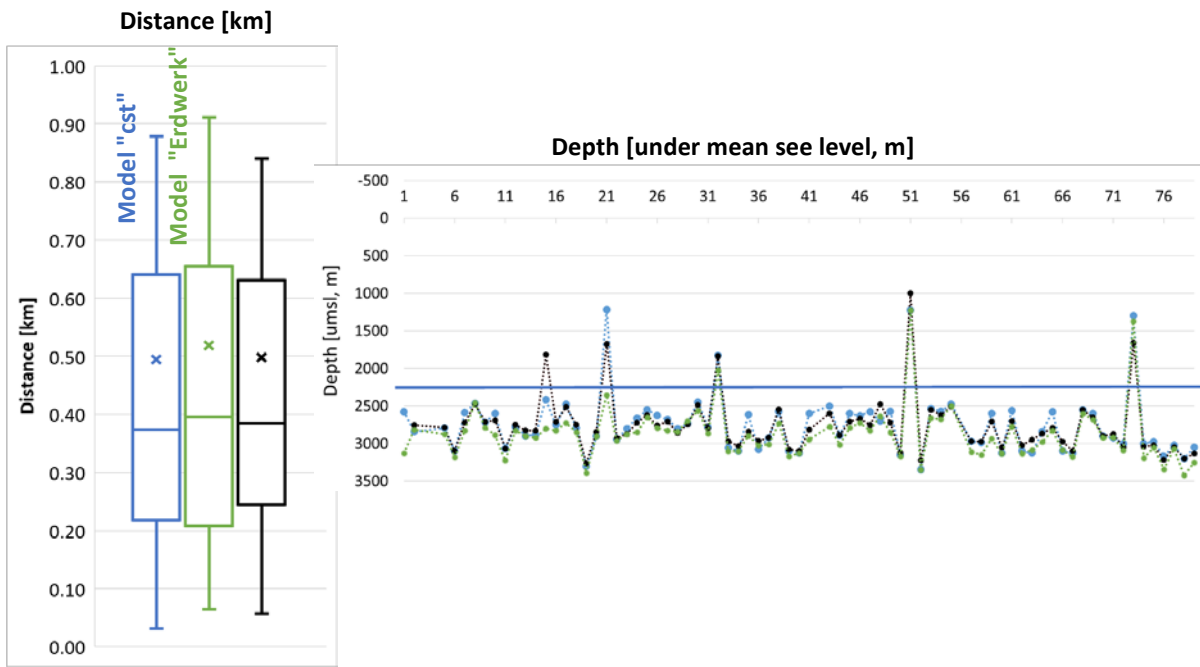
Figure 20: Comparison of location results obtained with three velocity models (denoted by different colors). Left-statistical representation of the distances between communicated and computed epicenters, for each considered velocity model. Right - differences in depths of hypocenters. The distribution of values shown in boxplots represents the variability in location results obtained for all considered events. The whiskers extend to the upper and lower quartile; the cross shows the mean value and the line the median of the series.
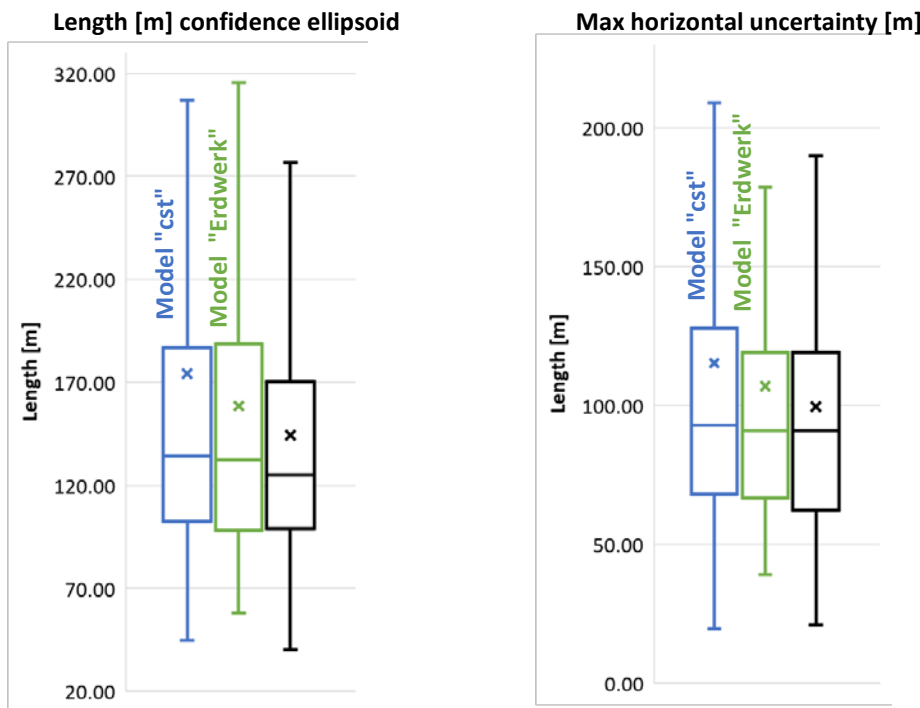
Figure 21: Comparison of velocity models (colors) based on the distribution of lengths of semi-major (left) and semi-minor (right) axis of 68% confidence ellipsoid. The distribution of values shown in boxplots represents the variability in location results obtained for all considered events. The whiskers extend to the upper and lower quartile; the cross shows the mean value and the line the median of the series.

Figure 22: Comparison of velocity models (colors) based on the distribution of root-mean-square (RMS) values of residuals at maximum likelihood (left) and on the distribution of station residuals (right). The distribution of values shown in boxplots represents the variability in location results obtained for all considered events. The whiskers extend to the upper and lower quartile; the cross shows the mean value and the line the median of the series.

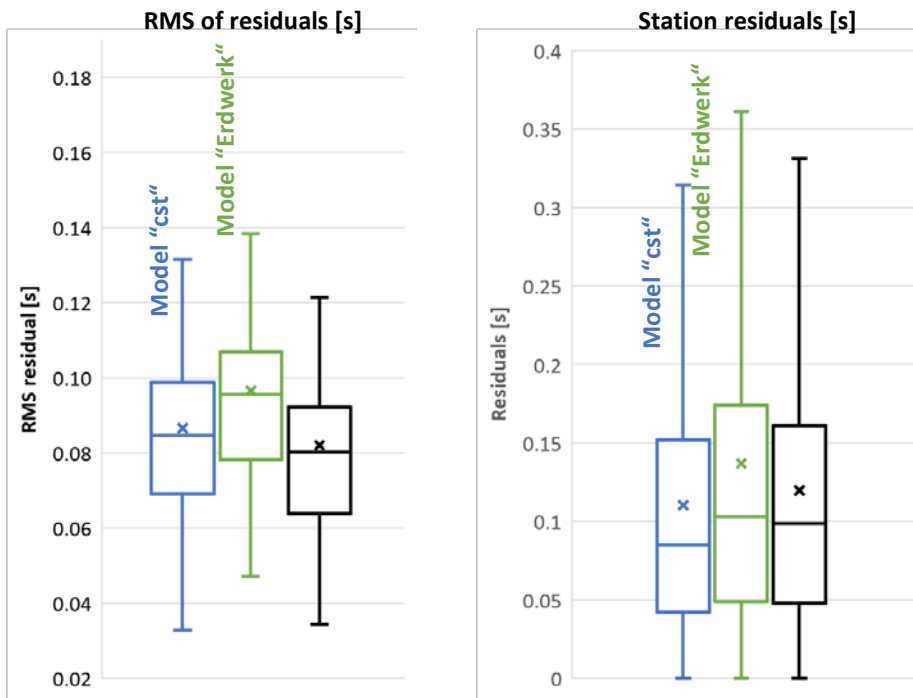**Table 9: List of cumulative delay for P and S phases at each station with associated standard deviation, for each of the tested velocity structure. The statistics are obtained from the 79 located events.**

Station name	Phase	Model 1		Model "Erdwerk"		Model "cst"	
		Cumulative delay [s]	Standard dev. [s]	Cumulative delay [s]	Standard dev. [s]	Cumulative delay [s]	Standard dev. [s]
BUCH	P	0.075	0.070	0.081	0.108	0.077	0.066
FORS	P	0.100	0.084	0.136	0.215	0.123	0.084
FRIE	P	0.082	0.153	0.128	0.101	0.101	0.162
MGS01	P	0.062	0.082	0.058	0.129	0.059	0.085
MGS02	P	0.009	0.092	0.011	0.212	0.008	0.082
MGS03	P	-0.001	0.205	0.020	0.130	0.017	0.204
MGS05	P	0.006	0.116	0.009	0.258	0.012	0.111
SIEM	P	0.081	0.074	0.088	0.099	0.055	0.072
UH3	P	0.020	0.091	0.008	0.147	0.016	0.087
WBRU	P	0.041	0.038	0.040	0.191	0.029	0.034
BUCH	S	-0.145	0.106	-0.163	0.207	-0.119	0.112
FORS	S	-0.108	0.125	-0.120	0.146	-0.068	0.128
FRIE	S	-0.120	0.158	-0.168	0.288	-0.075	0.154
MGS01	S	-0.088	0.111	-0.087	0.125	-0.062	0.108
MGS02	S	-0.144	0.086	-0.139	0.033	-0.129	0.082
MGS03	S	-0.164	0.127	-0.188	0.192	-0.126	0.122
MGS05	S	-0.289	0.147	-0.287	0.112	-0.256	0.146
SIEM	S	-0.085	0.102	-0.093	0.154	-0.123	0.109

Station name	Phase	Model 1		Model "Erdwerk"		Model "cst"	
		Cumulative delay [s]	Standard dev. [s]	Cumulative delay [s]	Standard dev. [s]	Cumulative delay [s]	Standard dev. [s]
UH3	S	-0.158	0.095	-0.189	0.106	-0.134	0.087
WBRU	S	-0.127	0.057	-0.132	0.058	-0.108	0.078

6.3 SUMMARY AND VELOCITY MODEL SELECTION

Considering the measurements obtained for the three tested velocity model, we observe:

- The velocity profile fitting more precisely the logging data (in black) yields better results in terms of residuals and location errors than the model fitting the Erdwerk dataset (in green).
- The blocky model gives more contrasted results than the one based on a linear evolution of velocities with depth.
- With the Model 1, relatively small time-residuals are obtained. The results are relatively consistent with GOF epicenters and VSP travel times.

We select the "gradient" velocity model for the south of Munich that closely fits the borehole data, i.e. that includes the decrease in velocity observed above Purbeck (results in black in previous figures). In view of the results, we conclude that Model 1 is the most suitable for event location and provides a more reliable description of the actual subsurface conditions.

7 INFLUENCE OF THE NETWORK GEOMETRY

Velocity models that do not reliably describe subsurface conditions can lead to erroneous location results. In this situation, the fact that the network of seismometers does not adequately cover the study area reinforces the bias in hypocenter determination. This situation is illustrated by locating the seismic catalogue using the onset times measured only on the five INSIDE stations. Hence, the hypocenters are obtained following the same workflow as for Figure 7, with the same velocity structure, but by removing the onset times measured on BayernNetz stations. The five INSIDE stations are all positioned northwest to the study zone (Figure 2).

Figure 23 shows the epicenters of events detected and located only with recordings from the five INSIDE stations. The locations are compared with the communicated epicenters as previously in Figure 7. The systematic North-West shift observed in the locations is indicative of the fact that most events detected during INSIDE are off centered in relation to the deployed network. Simultaneously, the location consistently results in shallower depth positions, as shown in Figure 24 that compares the depth inverted in both situations. The hypocenters obtained using solely INSIDE stations are systematically located above the Purbeck / Malm interface, highlighted in blue. This is indicative of biased results, as we expect the events to origin from the reservoir or the crystalline basement.

Using only INSIDE stations in the inversion of hypocenters introduces a significant bias, leading to considerably larger differences observed with the LMU data compared to those depicted in Figure 7, typically exceeding 1 kilometer.
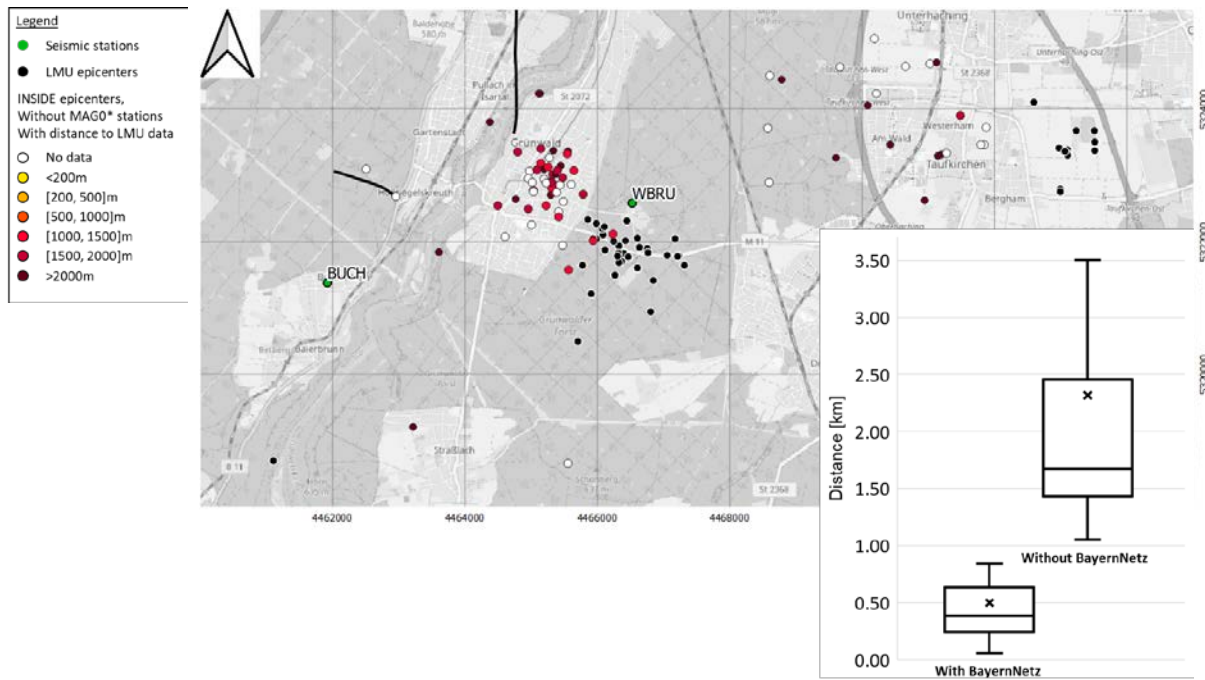
Figure 23: Same as Figure 7, with epicenters computed without using the arrival times measured at the public stations of the BayernNetz network. The boxplots on the lower-right corner show the distribution of distances to communicated epicenters in both cases: by using (left – "with") or by discarding (right – "without") the arrival-times measured at the public BayernNetz stations. The whiskers extend to the upper and lower quartile; the cross shows the mean and the line the median of the series.
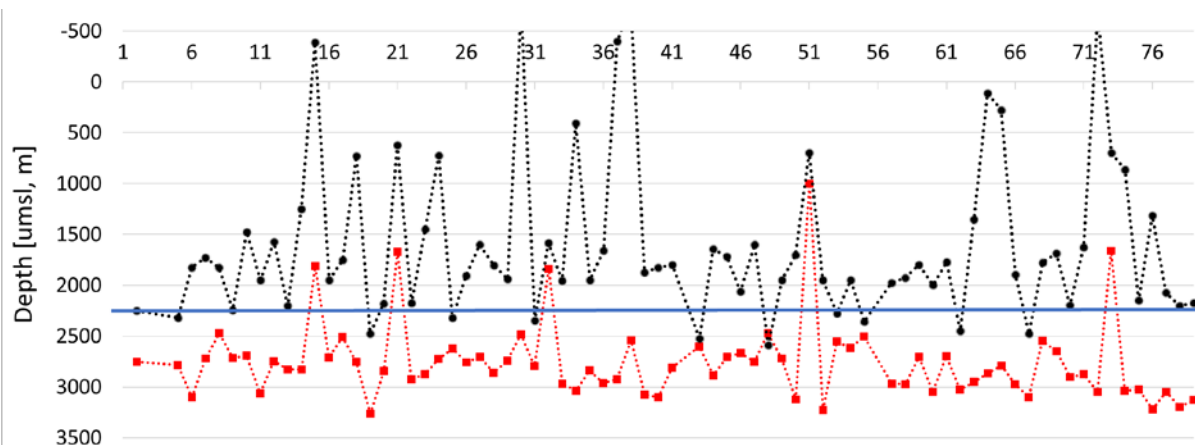
Figure 24: Hypocenter depth computed for the 79 events listed in Table 4. Black (respectively red) denotes the measurements obtained without using (with) the arrival times at the public stations of the BayernNetz. The blue line indicates the approximate depth of the Purbeck / Malm interface, which is indicative of the top of the geothermal reservoir.

Figure 25 shows differential travel times calculated by subtracting origin times from hypocenters computed with and without MAGS* stations. It shows that origins are systematically earlier (i.e., more recent origin times) when including the stations of the BayernNetz. This illustrates the trade off in the location procedure between the spatial (location) and temporal (origin time) aspect of the inversion problem.
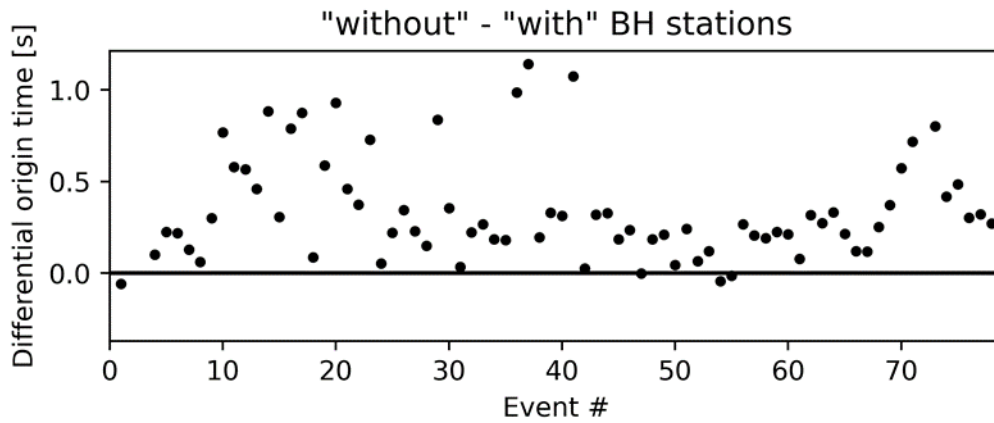
Figure 25: Difference between estimated origin times, when comparing the situation using only INSIDE stations and using a combination of INSIDE and BeyerNetz (BH) stations.

Removing the BayernNetz stations in the event location increases the relative weight of the velocity model between the INSIDE stations and the hypocenter. This analysis emphasizes the importance of having P- and S-wave velocity models that accurately reflect the true geological conditions between the seismic source and the receivers; especially as the stations-to-receiver distance increases and that the stations do not cover the study area.

8   OBSERVED AND MODELLED NETWORK SENSITIVITY

Figure 26: Simulated - detection capabilities from seismic noise recorded at the INSIDE stations. The map shows the minimum detectable magnitude, for events located at the geothermal reservoir level (2300 m umsl).

The usefulness and sensitivity of stations within a network can be analyzed from noise measurements. This aspect has been evaluated within the INSIDE project after the commissioning of the network and is the subject of a dedicated report (see report "Seismisches Netzwerk INSIDE: Aufbau und Inbetriebnahme", milestone M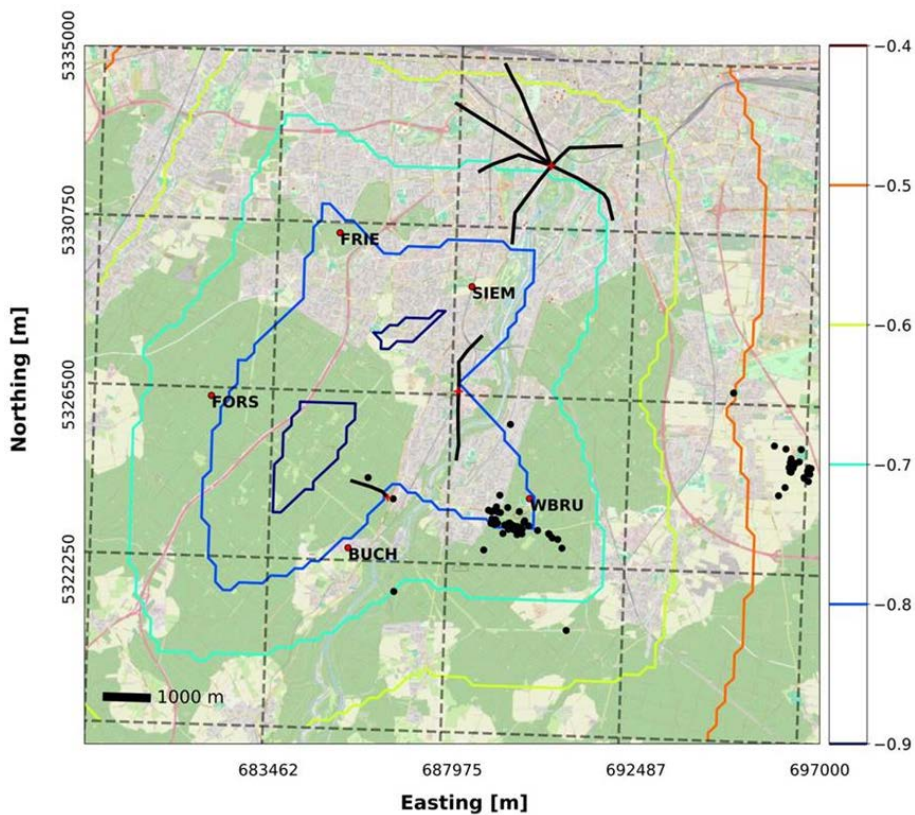1.2.3). The analysis of the ambient field, here ground vibrations recorded during one month, gives the possibility to simulate the capabilities of the network, in terms of detectable magnitudes. In Figure 26, we show the spatial distribution of minimal magnitude that could be detected at the level of the reservoir, focusing on the five INSIDE stations. The contours on the map are the projection of these values estimated at depth, on the surface. On the map, we read that the minimum magnitude lies between -0.7 and -0.8 for the area covered by the Oberhaching cluster. It is between -0.4 and -0.5 for the Unterhaching cluster.

We then compare the estimated capabilities to the minimum magnitude detected over the study area. We consider both major clusters previously identified, for which the minimum and maximum event magnitudes are detailed in Table 10.

Table 10: Observations – minimum and maximum local magnitude observed within each major cluster of events

	Minimum	Maximum
Unterhaching	-0.55	1.6
Oberhaching	-0.75	0.8

The consistency between the simulated and observed capabilities shows that the INSIDE network works as expected. It is in capacity to detect seismic events originating from the reservoir with a magnitude down to -0.8 under the surface covered by the 5 stations. However, very few events were detected during the time of the INSIDE project over this area.

9 SUMMARY

The INSIDE project aims to improve the understanding of induced seismicity and ground deformation associated with geothermal operations in the South German Molasse Basin and seismic monitoring is key in achieving this objective. The INSIDE seismic monitoring network consists of a range of instruments deployed across five sites. This includes four surface stations, one borehole station (SIEM), one Distributed Fiber Optic Sensing (DFOS) station collocated to the surface seismometer in Buchenhain, and a Mini-Array including nine geophones and installed at the same location as the borehole seismometer. This document focusses on the seismic monitoring results obtained from the network of seismometers, as a prerequisite for the comparison of recording methods and configurations (see associated report).

Data acquisition by the seismometer network was continuous, with occasional downtimes primarily affecting the FORS and FRIE stations. In comparison, data availability for the DAS station in Buchenhain was also impacted by hardware issues and GPS disconnections. The nine geophones of the mini-array rarely worked together due to logistical constraints.

The report presents a catalogue of 79 seismic events detected during the monitoring period. The detection workflow relied on a network coincidence trigger based on the STA/LTA algorithm and supported by a template matching approach. The methodology and results are provided for both

absolute and relative location of the seismic events. Analysis of the relocated seismicity did not reveal significant temporal trends in event locations or magnitude. The analysis identifies two significant clusters associated with the Unterhaching and Oberhaching sites, and a third cluster of only 2 events is identified near Pullach TH3. The results of the seismic monitoring shows that the network is working with a sensitivity to detection that fits the prediction, modelled based on noise measurements (see associated report). Thanks to the new stations installed within the project, it complements the BayernNetz operated by the Geophysical Observatory Fürstenfeldbruck (GOF), with a set of detected events that were not reported by GOF. In this regard, the WBRU station is particularly helpful and features high SNR due to its proximity to the Oberhaching geothermal site. However, the SIEM seismometer recordings do not contribute significantly to the detection of seismic events, despite the sensor being installed at a depth of around 180m, which is assumed to be linked to ground-sensor coupling issues.

The report presents an extensive analysis of the influence of the velocity model and of the network geometry on the location results. We test the hypothesis underlying the development of the velocity model, i.e. linear *versus* step-evolution of velocities with depth and increase *versus* decrease of velocities with depth in Liegende-Tonmergel. The analysis leads to the selection of the gradient velocity model closely fitting logging data. The location results lead to relatively small time-residuals. The measurements are also consistent with the GOF epicenters and VSP travel times. Comparing location results obtained with solely the INSIDE network (which poorly covers the Unterhaching and Oberhaching sites) with those obtained by including additionally the public stations of the BayernNetz highlights the importance of network coverage and accurate velocity models. We observe an offset ranging from 50 and 950 m with the GOF epicenters when including BayernNetz stations and using the developed velocity model. Excluding the BayernNetz stations results in a significant bias, shifting the locations westwards and to shallower depths.

In the future, the INSIDE network will successfully complement the existing BayernNetz network. The gradient velocity model developed in 3D is effective for locating events on the scale of the large study area. In future work, event location can be complemented by more refined models that describe the subsurface properties at a more local scale around the geothermal sites of interest and better fit local trends. In parallel, it is recommended to further refine the model by completing it with additional data acquisition campaigns. This would include planning VSP campaigns as part of future drilling projects, to tie in with active surface seismic campaigns.

10 METHODS

10.1 METHODS FOR EVENT DETECTION

This section describes the workflow applied to detect seismic events using the recordings of the five surface and borehole seismometer stations deployed within the INSIDE project. The outcomes are illustrated from the catalogue of events detailed in Table 4.

The recordings from the seismometer network are processed once per month to detect new seismic events, which implies that the data are not triggered in real time. The detection is based on a network coincidence trigger, itself based on a recursive STA/LTA algorithm (Trnkoczy, 2012; Withers et al., 1998). The algorithm uses the Obspy library (Beyreuther et al., 2010).The parameters of the STA-LTA routine are detailed in Table 11.

Table 11: STA-LTA triggering parameters

STA	0.3	Length of STA window [s]
LTA	3	Length of LTA window [s]
Threshold on	3.5	Threshold for trigger to turn on the trigger
Threshold off	1.5	Threshold for trigger to turn off the trigger
Coincidence sum	4	Minimum number of simultaneous individual triggers for triggering an event
Threshold on coincidence sum	7	Coincidence number necessary to consider a detected event as meaningful, without noticeable correlation with template waveforms
Threshold on normalized correlation coefficient with templates	0.7	Threshold above which detected events are considered as meaningful, provided a good correlation with available template waveforms

For increased sensitivity, the detection routine involves two steps. Firstly, a dense set of event is detected by using a relaxed threshold on the "coincidence sum" parameter, i.e. 4 simultaneous triggers (to be compared to the number of channels, 15). The detected events are then further analyzed to determine if they are potential seismic events. There are two possibilities for an event to be classified as such:

- The cumulative sum exceeds a stricter threshold. Here, we require a coincidence larger or equal to 7.
- Or the cumulative sum does not exceed the threshold, but there is a significant correlation between traces recorded at the trigger time and previously identified template waveforms. Here, we require a normalized correlation coefficient large or equal to 0.7.

The template waveforms are selected from all previously detected events. We retain the traces on which a significant SNR is observed and extract 2.5 s long waveforms after the onset time at the station.

After the described detection workflow, a quality control is performed on the final set of detected events to validate or reinterpret the detections. Visual inspections are carried out in the Pyrocko application "Snuffler".

Depending on the strength of the seismic signal with respect to the background noise (i.e., the signal-to-noise ratio, or SNR) and the possibility to pick the seismic phases with precision, the validated detections are further analyzed in view of a more precise description of the seismic source. This includes the location of the seismic source (see Section 10.2), and the evaluation of event magnitudes (local and moment magnitude).

For the location of seismic events, we require a minimum of three P- or S-wave onset times (measured at three different station). For local seismic monitoring, we consider that the picking of phases on a single channel is possible with a SNR exceeding 3. This approach is consistent with the theoretical analysis used to evaluate the detection capabilities of the network with noise recordings (see report "Seismisches Netzwerk INSIDE: Aufbau und Inbetriebnahme", milestone M1.2.3). The picking of phases is carried out manually in the Obspyck environment.

Onset times are measured using the recordings of the INSIDE network for all seismic events reported in Section 4. However, the INSIDE network is not adapted to locate event associated with the

Oberhaching and Unterhaching sites. As these events represent the vast majority of the detections observed since the commissioning of the monitoring network we complete the dataset with the recordings of the public stations of the BayernNetz (Department of Earth and Environmental Sciences, Geophysical Observatory, University of Munchen, 2001). This includes the five MAG0* stations (see Figure 1) and the UH3 station. In addition, the inverted source locations are compared to a reference catalogue provided by the Geophysical Observatory (Tobias Megies, LMU, according to internal discussion). To consolidate the dataset from the INSIDE network, data from the public station of the BayernNetz are downloaded locally through the IRIS client. The waveforms are included in the Obspyck picking workflow to measure P- and S- wave onset times.

10.2 METHODS FOR ABSOLUTE LOCATION

The Non-Lin-Loc (NLL) software package (Lomax et al., 2014, 2000) is used in combination with the onset-time measurements and a 3D velocity structure (see Report about velocity structure construction) to invert for the source location. The location procedure is based on the Oct-Tree grid-search algorithm (Lomax and Curtis, 2001). The latter recursively subdivides a 3D-space in child-cells, converging towards the region of maximum likelihood using a tree structure. The method has the advantage of producing a compact representation of the probability density function (PDF) with an importance-based sampling. All the available P- and S- wave onset times are used during location of individual events, which covers those obtained at the INSIDE and at the BayernNetz stations.

The absolute location is carried out on HPC and is combined with the creation of travel time maps in a single framework.

10.3 METHODS FOR RELATIVE LOCATION

We use the GrowClust3D software package for event relocation (Trugman et al., 2023). It is a Julia implementation of a software package for the relative relocation of earthquake hypocenters. GrowClust3D uses a clustering approach to relocate earthquake catalogs based on differential time data obtained from waveform cross-correlation.

The software package uses all possible event pairs from the seismic catalogue for event relative location. For a given pair of events, one input is the differential travel time at each station measuring both events, computed as the difference in travel times. A second input is the correlation coefficient between waveform slices extracted around measured onset-times, for a given station / phase. These input parameters are produced from the absolute catalogue using a python script "from_Hyp2Reloc.py".

The 3D software package is compatible with NLL travel time grids. Hence, we use, for the relocation, the same travel time maps than those generated for the event location using the NLL software package. This allows for self-consistency between absolute and relative relocation estimates.

The event relative location is carried out on the HPC and combined to the generation of velocity models, the creation of travel time maps and the event absolute location in a single sequence.

10.4 MAGNITUDE ESTIMATION

We estimate local magnitudes (M_L) and moment magnitudes (M_W) from the measured event location and stations recordings.

M_L is based on the amplitude of seismic waves. For a given event, we estimate local magnitudes at each station from the response of the instruments, the observed peak-to-peak amplitude and the time span from peak to peak. To evaluate local magnitudes, we use the Obspy library (Beyreuther et al., 2010) and the associated function (see link) based on the formalism introduced by (Bakun and Joyner, 1984).

Moment magnitude, denoted as M_w, is based on seismic moment, which is a measure of the total energy released during an earthquake. M_w takes into account the fault length, slip along the fault, and the material properties of the rocks involved. Moment magnitudes are more sophisticated but they represent a more comprehensive measure of earthquake size compared to local magnitude. The inversion is based on fitting a source model to the amplitude spectrum calculated at each station from the event recordings. An amplitude spectrum is obtained by applying Fourier transformation to the velocity recordings of 0.8 seconds duration, starting from the P-wave onset time. Modelled spectra are obtained from (Anderson and Hough, 1984). We use the model proposed by (Madariaga, 1976) to describe the fault dynamic and quantify the source parameters, including the seismic moment. The inversion procedure entails testing a range of potential model parameters and relies on a least squares regression approach. In this process, the fit between observations and modeled spectra is evaluated for a range of corner frequencies f_0 and values of amplitude plateau Ω_0.

11 BIBLIOGRAPHY

Anderson, J.G., Hough, S.E., 1984. A model for the shape of the fourier amplitude spectrum of acceleration at high frequencies. Bulletin of the Seismological Society of America 74, 1969–1993. https://doi.org/10.1785/BSSA0740051969

Azzola, J., Gaucher, E., 2024. Seismic Monitoring of a Deep Geothermal Field in Munich (Germany) Using Borehole Distributed Acoustic Sensing. Sensors 24, 3061. https://doi.org/10.3390/s24103061

Azzola, J., Thiemann, K., Gaucher, E., 2023. Integration of distributed acoustic sensing for real-time seismic monitoring of a geothermal field. Geothermal Energy 11, 30. https://doi.org/10.1186/s40517-023-00272-4

Bakun, W.H., Joyner, W.B., 1984. The *ML* scale in central California. Bulletin of the Seismological Society of America 74, 1827–1843. https://doi.org/10.1785/BSSA0740051827

Beyreuther, M., Barsch, R., Krischer, L., Megies, T., Behr, Y., Wassermann, J., 2010. ObsPy: A Python Toolbox for Seismology. Seismological Research Letters 81, 530–533. https://doi.org/10.1785/gssrl.81.3.530

Department of Earth and Environmental Sciences, Geophysical Observatory, University of Munchen, 2001. BayernNetz (BH) seismic network. International Federation of Digital Seismograph Networks. https://doi.org/10.7914/SN/BW

Lomax, A., Curtis, A., 2001. Fast, probabilistic earthquake location in 3D models using oct-tree importance sampling, in: 955. Geophys. Res. Abstr., pp. 10–1007.

Lomax, A., Michelini, A., Curtis, A., 2014. Earthquake Location, Direct, Global-Search Methods, in: Meyers, R.A. (Ed.), Encyclopedia of Complexity and Systems Science. Springer New York, New York, NY, pp. 1–33. https://doi.org/10.1007/978-3-642-27737-5_150-2

Lomax, A., Virieux, J., Volant, P., Berge-Thierry, C., 2000. Probabilistic Earthquake Location in 3D and Layered Models, in: Thurber, C.H., Rabinowitz, N. (Eds.), Advances in Seismic Event Location, Modern Approaches in Geophysics. Springer Netherlands, Dordrecht, pp. 101–134. https://doi.org/10.1007/978-94-015-9536-0_5

Madariaga, R., 1976. Dynamics of an expanding circular fault. Bulletin of the Seismological Society of America 66, 639–666. https://doi.org/10.1785/BSSA0660030639

Trnkoczy, A., 2012. Understanding and parameter setting of STA/LTA trigger algorithm, Bormann, P. (Ed.). ed, New Manual of Seismological Observatory Practice (NMSOP).

Trugman, D.T., Chamberlain, C.J., Savvaidis, A., Lomax, A., 2023. GrowClust3D.jl: A Julia Package for the Relative Relocation of Earthquake Hypocenters Using 3D Velocity Models. Seismological Research Letters 94, 443–456. https://doi.org/10.1785/0220220193

Withers, M., Aster, R., Young, C., Beiriger, J., Harris, M., Moore, S., Trujillo, J., 1998. A comparison of select trigger algorithms for automated global seismic phase and event detection. Bulletin of the Seismological Society of America 88, 95–106. https://doi.org/10.1785/BSSA0880010095